

Earth, Planets and Space

Simultaneous observation of auroral substorm onset in Polar satellite global images and ground-based all-sky images

--Manuscript Draft--

Manuscript Number:	EPSP-D-17-00305R4	
Full Title:	Simultaneous observation of auroral substorm onset in Polar satellite global images and ground-based all-sky images	
Article Type:	Full paper	
Section/Category:	Space science	
Funding Information:	Japan Society for the Promotion of Science (JP16K05568)	Dr Akimasa Ieda
	Japan Society for the Promotion of Science (JP26247082)	Dr Shinobu Machida
	Japan Society for the Promotion of Science (JP16H04057)	Dr Masahito Nosé
	Japan Society for the Promotion of Science (26610143)	Dr Masahito Nosé
	National Aeronautics and Space Administration (NNX15AI62G)	Dr Yukitoshi Nishimura
	National Science Foundation (AGS-1451911)	Dr Yukitoshi Nishimura
	Air Force Office of Scientific Research (FA9550-15-1-0179)	Dr Yukitoshi Nishimura
Abstract:	<p>Substorm onset has originally been defined as a longitudinally extended sudden auroral brightening (Akasofu initial brightening: AIB) followed a few minutes later by an auroral poleward expansion in ground-based all-sky images (ASIs). In contrast, such clearly marked two-stage development has not been evident in satellite-based global images (GIs). Instead, substorm onsets have been identified as localized sudden brightenings that expand immediately poleward. To resolve these differences, optical substorm onset signatures in GIs and ASIs are compared in this study for a substorm that occurred on December 7, 1999. For this substorm, the Polar satellite ultraviolet global imager was operated with a fixed filter (170 nm) mode, enabling a higher time resolution (37 s) than usual to resolve the possible two-stage development. These data were compared with 20-s-resolution green-line (557.7 nm) ASIs at Muonio in Finland. The ASIs revealed the AIB at 2124:50 UT and the subsequent poleward expansion at 2127:50 UT, whereas the GIs revealed only an onset brightening that started at 2127:49 UT. Thus, the onset in the GIs was delayed relative to the AIB and in fact agreed with the poleward expansion in the ASIs. The fact that the AIB was not evident in the GIs may be attributed to the limited spatial resolution of GIs for thin auroral arc brightenings. The implications of these results for the definition of substorm onset are discussed herein.</p>	
Corresponding Author:	Akimasa Ieda Nagoya university JAPAN	
Corresponding Author Secondary Information:		
Corresponding Author's Institution:	Nagoya university	
Corresponding Author's Secondary Institution:		
First Author:	Akimasa Ieda	

First Author Secondary Information:	
Order of Authors:	Akimasa Ieda
	Kirsti Kauristie
	Yukitoshi Nishimura
	Yukinaga Miyashita
	Harald U Frey
	Liisa Juusola
	Daniel Whiter
	Masahito Nosé
	Matthew O Fillingim
	Farideh Honary
	Neil C Rogers
	Yoshizumi Miyoshi
	Tsubasa Miura
	Takahiro Kawashima
	Shinobu Machida
Order of Authors Secondary Information:	
Response to Reviewers:	There was no reviewer comments.

[Click here to view linked References](#)

1
2
3
4
5
6
7
8
9
10
11
12
13
14
15
16
17
18
19
20
21
22
23
24
25
26
27
28
29
30
31
32
33
34
35
36
37
38
39
40
41
42
43
44
45
46
47
48
49
50
51
52
53
54
55
56
57
58
59
60
61
62
63
64
65

- 1 **Simultaneous observation of auroral substorm onset in Polar**
- 2 **satellite global images and ground-based all-sky images**

1
2
3
4
5 3 Akimasa Ieda¹ (Corresponding Author), ieda@nagoya-u.jp

6
7 Kirsti Kauristie², Kirsti.Kauristie@fmi.fi

8
9 Yukitoshi Nishimura^{3,4}, toshi@atmos.ucla.edu

10
11 Yukinaga Miyashita⁵, miyasita@kasi.re.kr

12
13 Harald U. Frey⁶, hfrey@ssl.berkeley.edu

14
15 Liisa Juusola², Liisa.Juusola@fmi.fi

16
17 Daniel Whiter⁷, d.whiter@soton.ac.uk

18
19 Masahito Nosé⁸, nose@kugi.kyoto-u.ac.jp

20
21 Matthew O. Fillingim⁶, matt@ssl.berkeley.edu

22
23 Farideh Honary⁹, f.honary@lancaster.ac.uk

24
25 Neil C. Rogers⁹, n.rogers1@lancaster.ac.uk

26
27 Yoshizumi Miyoshi¹, miyoshi@isee.nagoya-u.ac.jp

28
29 Tsubasa Miura¹, tsubasa@isee.nagoya-u.ac.jp

30
31 Takahiro Kawashima¹, takahiro0316@isee.nagoya-u.ac.jp

32
33 Shinobu Machida¹, machida@isee.nagoya-u.ac.jp

34
35
36 ¹Institute for Space-Earth Environmental Research, Nagoya University, Nagoya, Aichi,
37
38 Japan.

39
40 ²Finnish Meteorological Institute, Helsinki, Finland.

41
42 ³Department of Atmospheric and Oceanic Sciences, University of California, Los Angeles,
43
44 California, USA.

45
46 ⁴Department of Electrical and Computer Engineering and Center for Space Physics, Boston
47
48 University, Boston, Massachusetts, USA.

49
50 ⁵Korea Astronomy and Space Science Institute, Daejeon, South Korea.

51
52 ⁶Space Sciences Laboratory, University of California, Berkeley, California, USA.

53
54 ⁷School of Physics and Astronomy, University of Southampton, Highfield, Southampton,
55
56 UK.

57
58 ⁸Data Analysis Center for Geomagnetism and Space Magnetism, Graduate School of Science,
59
60 Kyoto University, Kyoto, Japan.

61
62 ⁹Space and Planetary Physics, Lancaster University, Bailrigg, Lancaster, UK.
63
64
65

1
2
3
4
5
6
7
8
9
10
11
12
13
14
15
16
17
18
19
20
21
22
23
24
25
26
27
28
29
30
31
32
33
34
35
36
37
38
39
40
41
42
43
44
45
46
47
48
49
50
51
52
53
54
55
56
57
58
59
60
61
62
63
64
65

5 **Abstract**

6 Substorm onset has originally been defined as a longitudinally extended sudden auroral brightening
7 (Akasofu initial brightening: AIB) followed a few minutes later by an auroral poleward expansion in
8 ground-based all-sky images (ASIs). In contrast, such clearly marked two-stage development has not
9 been evident in satellite-based global images (GIs). Instead, substorm onsets have been identified as
10 localized sudden brightenings that expand immediately poleward. To resolve these differences, optical
11 substorm onset signatures in GIs and ASIs are compared in this study for a substorm that occurred on
12 December 7, 1999. For this substorm, the Polar satellite ultraviolet global imager was operated with a
13 fixed filter (170 nm) mode, enabling a higher time resolution (37 s) than usual to resolve the possible
14 two-stage development. These data were compared with 20-s-resolution green-line (557.7 nm) ASIs at
15 Muonio in Finland. The ASIs revealed the AIB at 2124:50 UT and the subsequent poleward expansion
16 at 2127:50 UT, whereas the GIs revealed only an onset brightening that started at 2127:49 UT. Thus,
17 the onset in the GIs was delayed relative to the AIB and in fact agreed with the poleward expansion in
18 the ASIs. The fact that the AIB was not evident in the GIs may be attributed to the limited spatial
19 resolution of GIs for thin auroral arc brightenings. The implications of these results for the definition of
20 substorm onset are discussed herein.

21 **Keywords**

22 substorm, auroral breakup, aurora, substorm onset, global images, all-sky images

23 **Introduction**

24 A substorm refers to the explosive release of stored energy in the magnetotail (e.g., *Akasofu* 1977). It
25 is necessary to identify substorm onsets with an accuracy of at least a few minutes to determine the
26 triggering mechanism of the substorm, such as magnetic reconnection in the magnetotail. Substorm
27 onsets have often been identified with a sudden auroral brightening in both satellite-based global images
28 (GIs) and ground-based all-sky images (ASIs). Thus, this sudden brightening should exhibit similar
29 features in both GIs and ASIs. However, the shape of the observed sudden brightening actually differs
30 between the two image types.

1
2
3
4
5
6
7
8
9
10
11
12
13
14
15
16
17
18
19
20
21
22
23
24
25
26
27
28
29
30
31
32
33
34
35
36
37
38
39
40
41
42
43
44
45
46
47
48
49
50
51
52
53
54
55
56
57
58
59
60
61
62
63
64
65

31 The substorm concept is a comprehensive understanding of the auroral breakup phenomenon. Auroral
32 breakup used to refer to a sudden and intense increase in the brightness and motion of an aurora in
33 the polar ionosphere (e.g., *Elvey* 1957; *Akasofu* 1963). *Akasofu* (1964) captured auroral breakup images
34 using widely distributed ground all-sky cameras with a time resolution of 1 min. He found breakup-
35 associated new features and termed them collectively as a substorm. In particular, he identified the stage
36 in which the sudden auroral brightenings are wide in longitude as initial brightening (IB; Figure 1). It
37 should be noted that the IB is recognized as wide when considered on a time scale of a few minutes. On
38 much shorter time scales, the same IB may appear localized at the very beginning and expand quickly
39 in longitude (e.g., *Akasofu* 2012). The auroral bead phenomenon (e.g., *Liang et al.* 2008) is presumably
40 one such type of detailed feature of this wide brightening.

41 The IB does not merely imply the “first” observed brightening; it also describes the time of the substorm
42 onset (e.g., *Akasofu et al.* 2010). We refer to this phenomenon as Akasofu IB (AIB) in the present study
43 to avoid confusion. Accordingly, when a substorm onset is specifically identified on the basis of AIB, this
44 type is referred to as “Akasofu substorm onset”. The AIB is followed by poleward expansion of the aurora
45 a few minutes later in the original substorm model (*Akasofu* 1964). That is, *Akasofu* (1964) found that
46 the auroral breakup phenomenon (e.g., *Akasofu* 1963) begins with a two-stage development. The term
47 “auroral breakup” has been used in various contexts. In the present study, we define auroral breakup as
48 an auroral brightening immediately followed by poleward expansion. In this context, auroral breakup is
49 delayed as compared with the Akasofu substorm onset.

50 In contrast to *Akasofu* (1964), the substorm onset is not recognized as being elongated along longitudes
51 but is instead localized in statistical studies of GIs as follows. *Frey et al.* (2004); *Frey and Mende*
52 (2006) identified substorm onsets by “a clear local brightening of the aurora” within GIs observed by
53 the far ultraviolet imager (FUV) onboard the Imager for Magnetopause-to-Aurora Global Exploration
54 (IMAGE) satellite. *Liou* (2010) identified substorm onsets by “a sudden brightening of the aurora” within
55 GIs observed by the ultraviolet imager (UVI) onboard the Polar satellite. Practically, *Liou* (2010) first
56 identified an auroral bulge and then traced it back in time to identify its original instance and location.
57 Thus, the sudden brightening appears to have been recognized as relatively localized and immediately
58 followed by poleward expansion.

59 This localized onset in GIs may be confused as corresponding to the localized brightening observed in high
60 time-resolution ASIs of a few seconds. However, the longitudinally localized brightening in such ASIs

1
2
3
4
5
6
7
8
9
10
11
12
13
14
15
16
17
18
19
20
21
22
23
24
25
26
27
28
29
30
31
32
33
34
35
36
37
38
39
40
41
42
43
44
45
46
47
48
49
50
51
52
53
54
55
56
57
58
59
60
61
62
63
64
65

61 expands quickly in the east–west direction (e.g., *Liang et al.* 2008) to form a longitudinally extended
62 brighter aurora (i.e., AIB) before the poleward expansion. Because even such a longitudinally extended
63 aurora is not mentioned in these onset identifications made with GIs, the initially less intense localized
64 brightening in ASIs is not likely evident in GIs. In summary, substorm onsets in GIs are not likely to
65 correspond directly to the Akasofu substorm onsets in ASIs.

66 Because GIs have limited sensitivities compared with ASIs, small or weak signatures are not evident in
67 them. This widely established caveat implies that the time of the observed first brightening is expected
68 to be delayed in GIs compared with that in ASIs. In contrast, the possible delay of GI-onsets with respect
69 to ASI-onsets has been expected to be small, at less than ~ 1 min (e.g., *Liou* 2010). Moreover, substorm
70 onsets in GIs are simultaneous or even earlier than Pi2 pulsations (*Liou et al.* 1999). Thus, the impact
71 of the caveat on the identification of substorm onset time in GIs may not be significant.

72 This possible delay should be clarified by using simultaneous ASI and GI observations. The onsets often
73 begin outside ASI field-of-view (e.g., *Shiokawa et al.* 2005; *Yago et al.* 2007). Three fortunate cases with
74 onsets inside the ASI field-of-view have been reported (*Tagirov et al.* 1998; *Bristow et al.* 2003; *Donovan*
75 *et al.* 2006). *Tagirov et al.* (1998) and *Bristow et al.* (2003) recognized that the onsets are simultaneous
76 between ASIs and GIs on a time scale of 1 min. In contrast, *Donovan et al.* (2006) suggested that a
77 GI-onset is delayed by a few minutes. This delay is comparable to the time resolution (2 min) of the
78 IMAGE satellite FUV images and thus is not conclusive.

79 Because the Polar/UVI usually changes filters (e.g., *Tagirov et al.* 1998; *Bristow et al.* 2003), detailed
80 comparisons with ASIs within 3 min are generally difficult. However, the Polar/UVI is sometimes operated
81 under the fixed-filter mode. This mode enabled us to compare simultaneous GIs and ASIs with a practical
82 time resolution of less than 1 min for the first time.

83 The purpose of the present study is to clarify the difference in the observed substorm onset between
84 ASIs and GIs. Compared with GIs, the regional images from the Reimei satellite provide more consistent
85 timing information with ASIs (*Frey et al.* 2010; *Zou et al.* 2010). In the present study, “GIs” specifically
86 refer to images with a practical spatial resolution of ~ 50 km or slightly worse, such as Polar/UVI or
87 IMAGE/FUV images. These GIs were used to construct extensive substorm onset lists (*Frey and Mende*
88 2006; *Liou* 2010) that are publically available. Thus, substorm onsets identified in these GIs are practically
89 standard references and have been further compared widely with other signatures, particularly with tail
90 reconnection (e.g., *Baker et al.* 2002; *Kepko et al.* 2004; *Miyashita et al.* 2009). New results on substorm

1
2
3
4
5 91 onsets with ASIs should be compared with past results with GIs to gain a comprehensive understanding.
6
7 92 Thus, it is critical to clarify the difference between ASIs and GIs. In particular, we aim to understand
8
9 93 the absence of the two-stage development in GIs.
10
11 94 Accordingly, we suggest that substorm onsets that are identified using solely GIs do not necessarily cor-
12
13 95 respond to the Akasofu substorm onset in ASIs; rather, they correspond to the subsequent poleward
14
15 96 expansion. We will also show that traditional geomagnetic bays and mid-latitude Pi2 pulsations corre-
16
17 97 spond to poleward expansion rather than Akasofu substorm onset. These results require an update of the
18
19 98 interpretation of the time difference between the substorm onset and reconnection signatures reported in
20
21 99 previous studies.

100 **Data Set**

101 **Polar Satellite Global Images**

102 The Polar satellite ultraviolet imager (UVI) (*Torr et al. 1995*) provides global imaging of auroras. UVI
103 GIs are captured in the N₂ Lyman-Birge-Hopfield long (LBHL, ~170 nm) and short (LBHS, ~150 nm)
104 wavelengths and the OI ~130.4 nm and ~135.6 nm wavelengths. In particular, the LBHL images monitor
105 the energy flux of precipitating keV-range electrons (e.g., *Lummerzheim et al. 1997*) and thus can be
106 compared with green-line (557.7 nm) ASIs during substorms. The LBHS images are less useful for this
107 purpose because LBHS emissions are absorbed by the atmosphere en route to the imager, and this
108 absorption depends on the average energy of precipitating auroral electrons. The UVI captures four or
109 five images in each 184-s cycle. The filter and the exposure period usually vary during this 3-min cycle;
110 thus, the practical time resolution is usually 3 min for the same filter and exposure.

111 In the present study, the UVI captured images with a fixed wavelength (LBHL) and exposure mode at
112 36.8 s, which enabled a higher practical time-resolution of 36.8 s than the usual 3 min. This 37-s resolution
113 is expected to be marginally sufficient for resolving the two stages of the substorm onset sequence, which
114 are presumably separated by a few minutes. The spatial resolution (i.e., 1 pixel) of images (200 × 228
115 pixels) is ~37 × 31 km when viewed vertically from the Polar satellite with its apogee of 9R_E. Practically,
116 UVI images are smeared by approximately ±5 pixels owing to satellite-spin-associated wobbling (e.g.,
117 *Germany et al. 1998; Frank et al. 2001a*). The emission altitude was assumed to be 120 km from the
118 ground. Slant path brightness enhancements were corrected by using an empirical model similar to a
119 cosine curve (e.g., *Germany et al. 1998*). The emission brightness was converted to the energy flux of

1
2
3
4
5 120 the precipitating electrons that cause auroras by using 130 R per mW m^{-2} , referring to the results of
6
7 121 *Galand and Lummerzheim (2004)*.

8
9 122 Figure 2a1 shows an example of the UVI image in the raw charged couple device (CCD) coordinates with
10
11 123 an overlaid geographical map. The magnetic coordinates (Figure 2a2) have often been used to show GIs
12
13 124 in previous substorm studies. We calculated the magnetic latitude (MLAT) and longitude (MLON) in
14
15 125 degrees and the magnetic local time (MLT) in hours of the modified magnetic apex coordinates (*Richmond*
16
17 126 1995) for a reference altitude of 110 km using the IGRF-12 (*Thebault et al. 2015*) model.

127 **All-sky Images at Muonio (65 MLAT)**

128 The satellite images were compared with ASIs observed at Muonio (MUO: 64.6 MLAT, 105.2 MLON,
129 68.02°N, 23.53°E) in Lapland, Finland (e.g., Figures 2b1 and 2b2). The red circle in Figures 2b2 and
130 2a1 with a diameter of ~ 1000 km roughly indicates the field-of-view of the imager. This intensified CCD
131 all-sky camera is maintained by the Finnish Meteorological Institute (e.g., *Syrjäsuo et al. 1998; Sangalli*
132 *et al. 2011; Partamies et al. 2015*).

133 We used the green-line (557.7 nm) images captured every 20 s with an exposure time of 1 s. Figure 2b1
134 shows an example image in raw (CCD) coordinates. The 512×512 pixel images correspond to ~ 1 km
135 resolution overhead at an assumed emission altitude of 110 km. These geodetic coordinates (Figure 2b2)
136 have often been used to show ASIs in previous substorm studies.

137 **Observations**

138 **Satellite-Based Global Images**

139 Figure 3a shows the time sequence of Polar/UVI images in the MLT–MLAT polar coordinates. An
140 auroral brightening was first observed in the panel labeled in red at 2128:07 UT, which is mid-point of
141 the 36.8-s exposure time. The brightening was located around [23.2 MLT, 64.6 MLAT] as indicated by
142 the red circle. The time of the previous image was 2127:30 UT, just prior to the brightening event. We
143 consider the average of these two times, 2127:49 UT, as the beginning of the auroral brightening event.

144 This brightening appears to be localized at the beginning of the event and was immediately followed by
145 poleward expansion, as shown in later panels. These are typical signatures of auroral breakup, or substorm
146 onset, in GIs (e.g., *Liou et al. 2000; Frey et al. 2004*). This result is also shown in the auroral keogram
147 (Figure 3b), where the onset at 2127:49 UT is marked by a solid vertical line. No other brightenings
148 were evident before the onset, as also indicated by the average of the keogram data between 62 and

1
2
3
4 149 70 MLAT (Figure 3c), particularly around 3 min (dashed vertical line) before the onset. Because the
5
6 150 possible two-stage development was not identified, it is unclear solely from the GIs whether this substorm
7
8 151 onset is the Akasofu substorm onset.
9

10 152 **Ground-Based All-Sky Images**

11
12 153 In contrast, AIB was observed in the ground ASIs (Figures 4 and 5) captured at the MUO station. Figure
13
14 154 4 shows the time sequence of full-time 20-s resolution images. Figure 5a shows three selected images that
15
16 155 represent moments during the quiet time, initial brightening, and poleward expansion. A brightened
17
18 156 auroral arc is evident in the 2126:20 UT image in Figures 4 and 5a, but it is subjective to determine
19
20 157 precisely when it began. Tracing this arc back in time starting at 2126:20 UT, we determined that the
21
22 158 arc brightening began at the 2125:00 UT image in Figure 4. This detailed selection of the start time is
23
24 159 moderately supported by the auroral keogram (Figure 5b) and by the auroral brightness near the onset
25
26 160 location (Figure 5c), which shows a small enhancement in its increase rate.
27

28
29 161 However, faint spots appear before 2125:00 UT in Figure 4. In particular, a spot at (23.18 MLT, 64.6
30
31 162 MLAT) near the onset MLT in the 2124:00 UT panel may be another possible candidate for the start
32
33 163 of the brightening. Thus, the selection of the 2125:00 UT image as the first brightening is subjective for
34
35 164 approximately 1 min. The auroras show faint azimuthally separated structures near the onset MLT, e.g.,
36
37 165 2124:40 UT and 2126:20 UT panels. These structures are presumably consistent with auroral beading
38
39 166 (e.g., *Donovan et al.* 2006; *Liang et al.* 2008), although their signals are weak in this particular event.
40

41
42 167 The first brightening identified above was centered at [23.2 MLT, 64.6 MLAT] in the 2125:00 UT image and
43
44 168 spanned approximately between 22.8 and 23.6 MLT in the 2126:00 UT image. Because this brightening
45
46 169 occurred simultaneously within a few minutes across a wide longitude, it can be interpreted to be the
47
48 170 AIB that was used to define the substorm onset by *Akasofu* (1964). It should be noted that we do not
49
50 171 specifically require the AIB to be as wide as those illustrated in *Akasofu* (1964) and *Akasofu et al.* (2010),
51
52 172 which span 4-6 h in MLT and would be typically too wide before the poleward expansion. Because the
53
54 173 original images were captured at 20-s intervals, we assumed that the AIB began at 2124:50 UT, 10 s
55
56 174 before 2125:00 UT.
57

58
59 175 The brightened arc shows a small split at 23.1 MLT in the 2127:40 UT image, but the poleward expansion
60
61 176 has not yet started in this image and in the keogram. The poleward expansion actually begins in the
62
63 177 next image, at 2128:00 UT, when the bright part (22.8–23.5 MLT) of the auroral arc began to split in
64
65 178 the northern direction. The resultant poleward arc expanded further poleward, as shown in the 2129:00

1
2
3
4 179 UT panel. We assumed that this poleward expansion began at 2127:50 UT, 10-s before 2128:00 UT. An
5
6 180 associated auroral brightening occurred simultaneously or in the previous image at 2127:40 UT, depending
7
8 181 on the subjectivity. Because this second brightening was followed immediately by the poleward expansion,
9
10 182 it is considered in the present study to be an auroral breakup.
11
12 183 In summary, the AIB was identified at 2124:50 UT with a subjectivity of approximately 1 min. *Mende*
13
14 184 *et al.* (2009) also reported that AIB can be too gradual to identify within ~ 10 -s accuracy. The increasing
15
16 185 rate of auroral brightness was approximately constant during the AIB (Figure 5c). The poleward
17
18 186 expansion was identified at 2127:50 UT, which is delayed from the AIB by at least 2 min and most
19
20 187 likely 3 min. Thus, the two-stage development was evident in the ASIs.
21
22

23 188 **Comparisons of Ground and Satellite Images**

24
25 189 Figure 6 shows simultaneous comparisons of ground and satellite images. Figure 6a shows ground ASIs
26
27 190 observed at MUO, projected in the geodetic coordinates. These ASIs were selected with 40–180 s
28
29 191 separations to represent the observed instances (a1) before onset, (a2) at the start of the AIB, (a3
30
31 192 and a4) during the AIB, (a5) at the start of the poleward expansion, and (a6) during the poleward
32
33 193 expansion.
34
35

36 194 Figure 6b shows the corresponding Polar UVI images for the same fixed area as that in Figure 6a. Each
37
38 195 image was selected to correspond to an ASI (Figure 6a) within 7 s. A comparison of Figures 6a and 6b
39
40 196 reveals the poleward expansion in the ASIs (a5 and a6) was simultaneously observed in the GIs (b5 and
41
42 197 b6), although the GIs appear smeared by satellite-spin-associated wobbling. In contrast, the AIB in the
43
44 198 ASIs (a2, a3, and a4) was not evident in the corresponding GIs (b2, b3, and b4).
45
46

47 199 These characteristics were also observed in the keograms (Figure 7), where slices of images at 23.2 MLT
48
49 200 between 62 and 68 MLAT are shown. Again, poleward expansion was observed at about 2127:50 UT both
50
51 201 in the (a) ASIs and (b) GIs. In contrast, the AIB (i.e., Akasofu substorm onset), which was observed at
52
53 202 2124:50 UT in the ASIs, was not evident in the GIs until the poleward expansion began.
54

55 203 In summary, the counterpart of the AIB was not evident in the GIs. Consequently, the observed first
56
57 204 brightening in the GIs corresponded to the second brightening in the ASIs (i.e., poleward expansion).
58
59 205 Therefore, we suggest that the substorm onsets in the GIs and ASIs represent different stages of substorms,
60
61 206 particularly when these onsets are identified independently (e.g., Figures 3 and 4).
62
63
64
65

Solar Wind and Geomagnetic Indices

Figure 8 shows the solar wind and geomagnetic indices obtained from the Operating Missions as Nodes on the Internet (OMNI) (King and Papitashvili 2005) 1-min resolution data. The north-south component of the interplanetary magnetic field (IMF) was weakly southward between 0 and -3 nT from 2054 UT, or about 30 min prior to the AIB, to 2145 UT. The dawn-dusk component and the magnitude of IMF were relatively strong during this interval, at 6 nT duskward. The solar wind speed was relatively high at 600 km/s, although the plasma density was relatively low at $2/\text{cm}^3$, resulting in a normal dynamic pressure at 2 nPa.

The geomagnetic condition was moderately disturbed during the 2-h period, as shown by the Kp index (3+ to 3) and $SYM-H$ indices (\sim -30 nT). This disturbed interval belonged to a co-rotation interaction region-type weak (peak \sim -40 nT) magnetic storm that began four days prior at around 9 UT on December 3, 1999 (not shown). The AL index began to develop at 2129 UT (Figure 8), 1 min after the poleward expansion, and 4 min after the Akasofu substorm onset in the ground ASIs (Figure 7). The AL was -127, -128, and -245 nT at 2127, 2128, and 2129 UT, respectively, and reached its peak value of -355 nT at 2134 UT.

Negative Bays in the Ground Magnetic Field

Substorm onsets are also traditionally identified by using negative bays, positive bays, and Pi2 pulsations in ground magnetic field data. Figure 9 shows the negative bays with the 10-s resolution ground magnetic field data obtained from the International Monitor for Auroral Geomagnetic Effects (IMAGE) project (e.g., Viljanen et al. 1995; Tanskanen 2009). Figure 9a shows the northward (X), eastward (Y), and downward (Z) components of all available data in the geomagnetic coordinates. The Kiruna station (KIR: 64.6 MLAT, 102.7 MLON) was located at 23.4 MLT at the time of the AIB (2124:50 UT, the first red line). This location was close (Figure 9d) to the AIB centered at [23.2 MLT, 64.6 MLAT]. However, no significant magnetic variations were detected at KIR and at other stations at the time of the AIB.

In contrast, the poleward expansion (Figures 4 and 5) that began at 2127:50 UT (the second red line) was accompanied by decreases up to \sim 400 nT in the X component. The negative bays began around 2128 UT at the KIR and MUO stations near the onset MLAT, where the bays weakened temporarily after 2129 UT, presumably because the current center had moved poleward. The negative bay was more clearly observed just north (65.2–65.8°: ABK and KIL) of the onset MLAT (64.6°). Stations at higher latitudes (66.3–66.5°: AND and TRO) detected sharp negative bays 1 min later at 2129 UT, and detected

1
2
3
4
5 237 the largest decrease (~ 400 nT) among all stations at 2130 UT.

6
7 238 These magnetic field data were used to infer the equivalent electric current at an altitude of 110 km
8
9 239 by using the method described in *Juusola et al.* (2016). We first derived the two-dimensional maps
10
11 240 (not shown) of the equivalent current and then focused on the KIR station meridian at 103° magnetic
12
13 241 longitude, which was typically 0.2 h east of the auroral onset MLT center at 23.2 h. Figure 9b shows
14
15 242 the time evolution of the inferred equivalent current intensity at this longitude. The equivalent current
16
17 243 intensified around the time of the auroral poleward expansion, at 2127:50 UT. This intensification began
18
19 244 around the auroral onset MLAT, at 64.6° , and then expanded poleward; these results are consistent with
20
21 245 the latitudinal dependences of the observed magnetic variations shown in Figure 9a.

22
23 246 The major negative bay of ~ 400 nT beginning at 2128 UT in Figure 9a is considered to be a traditional
24
25 247 substorm onset signature in the present study. However, it should be noted that much smaller variations
26
27 248 are visible when the vertical scale is changed (Figure 9c). Decreases in X began at 2124 UT near the
28
29 249 onset latitude, ~ 15 nT at KIR and ~ 20 nT at MUO, corresponding to the weak enhancement in the
30
31 250 equivalent current intensity at 2124 UT (Figure 9b). These may be associated with the AIB (2124:50 UT
32
33 251 about ± 1 min), although it would be too weak to be identified conventionally as a substorm onset.

34 35 36 252 **Positive Bays and Pi2 Pulsations**

37
38 253 Figure 10 shows the 1-s resolution ground magnetic field data obtained through the Sub-Auroral Mag-
39
40 254 netometer Network (SAMNET) project (e.g., *Yeoman et al.* 1990), where stations below 60 MLAT were
41
42 255 selected. Positive bays in the X component were evident at HAN, NUR, and KVI stations near the
43
44 256 onset MLT, at 23.2 h. These positive bays started at about 2128:50 UT, which is ~ 1 min later than the
45
46 257 poleward expansion but 4 min later than the Akasofu substorm onset.

47
48 258 Simultaneously, magnetic pulsations began at these stations. The amplitude was approximately 3 nT
49
50 259 with a periodicity of ~ 50 s inside the Pi2 range, at 40–150 s. Thus, the mid-latitude Pi2 pulsations were
51
52 260 observed in association with the poleward expansion. Associated Pi2 pulsations were observed at other
53
54 261 stations (GML, BOR, and YOR), although their beginnings were less clear.

55
56
57 262 It should be noted that we concentrated on Pi2 pulsations at mid-latitudes, where no aurora was observed
58
59 263 in the GIs (Figure 3a). Such Pi2s represent global magnetic variations and thus have been traditionally
60
61 264 used as a substorm onset indicator. At auroral latitudes, Pi2-range variations may be observed at the
62
63 265 time of the IB if the observatory is coincidentally located at the right place. However, the temporal and
64
65 266 spatial variations of such auroral-latitude Pi2s are well correlated with local auroras (e.g., *Rae et al.* 2009).

1
2
3
4 267 Thus, the implications of such auroral-latitude Pi2s differ from the lower-latitude Pi2s. Although the
5
6 268 global variation component may be included in the Pi2-range variation at auroral latitudes, its extraction
7
8
9 269 is difficult in the presence of auroras.

10 270 In summary, the geomagnetic signatures of the substorm onset were observed, including the start of
11
12 271 development in AL, negative bay, positive bay, and mid-latitude Pi2 pulsation. Such signatures began
13
14
15 272 at about 2128–2129 UT, which is 0–1 min after the poleward expansion at 2127:50 UT but 3–4 min
16
17 273 after the AIB at 2124:50 UT. Thus, these signatures do not likely correspond to the AIB; rather, they
18
19 274 are more likely to be poleward expansion. The absence of significant geomagnetic responses to the AIB
20
21 275 was also reported by *Nishimura et al. (2012)*, *Lyons et al. (2013)*, and *Ieda et al. (2016)*. *Lyons et al.*
22
23 276 *(2013)* further concluded that significant geomagnetic variations correspond to post-onset streamers from
24
25 277 the poleward boundary of the auroral bulge. This detailed correspondence was difficult to confirm in
26
27 278 this particular event, with the limited time resolution. Therefore, we conclude simply that significant
28
29 279 geomagnetic variations correspond to poleward expansion.

30 31 32 33 34 280 **Discussion**

35
36 281 In the present case study, two distinct auroral brightenings were observed in ground ASIs, as expected: the
37
38 282 AIB and the following poleward expansion a few minutes later. This two-stage development is consistent
39
40 283 with the classic Akasofu substorm onset (*Akasofu 1964*) and presumably corresponds to two different
41
42 284 physical mechanisms.

43
44 285 In contrast, the AIB, which was observed in the ASIs, was not evident in the GIs, as illustrated in Figure
45
46 286 11. Consequently, the identified first brightening in the GIs corresponded to the second brightenings in
47
48 287 the ASIs (i.e., the poleward expansion). In this section, we discuss these differences between ASIs and
49
50 288 GIs, including time delay, causes, implications for the onset definitions, and impacts on the reconnection
51
52 289 timing.

53 54 55 290 **Time delay of Substorm Onsets Between Ground and Satellite Images**

56
57 291 In the present study, the substorm onset identified by using GIs was delayed from the ASI data by 3 min.
58
59 292 This delay corresponds to the time difference between the AIB and the poleward expansion and thus
60
61 293 corresponds to the duration of the first stage (Figure 1-1) of the substorm expansion phase in *Akasofu*
62
63 294 *(1964)* of a few minutes. This Stage 1 often includes auroral rays (*Akasofu 1964*). We believe that auroral
64
65 295 rays and auroral beads are different views of the same auroral structure and that both can be recognized

1
2
3
4
5 296 as detailed features of a longitudinally wide brightening (i.e., AIB in Figure 11).
6
7 297 The duration of the AIB in the ASIs was 2.5 min (*Rae et al.* 2009), a few minutes (*Mende et al.* 2009), and
8
9 298 7 min (*Motoba et al.* 2014) in previous case studies. The duration was 1–2 min on average and extended
10
11 299 to 7 min in a statistical study (*Nishimura et al.* 2016). Thus, large diversity occurs in the identified
12
13 300 delays/durations (~ 1 –7 min). In the present discussion, we assumed that the time delay is typically a
14
15 301 few minutes.

16
17 302 It is currently difficult to comprehensively understand this diversity, although a clue may be that the AIB
18
19 303 tends to have a short duration when it intensifies rapidly (*Nishimura et al.* 2016). Practically, precursor
20
21 304 brightenings are often observed prior to the AIB (e.g., *Ieda et al.* 2016). It is sometimes difficult to
22
23 305 determine whether such a brightening is the AIB or a precursor, particularly when it does not decay
24
25 306 significantly, leading to subjectivity in the duration of the AIB. Substorm onsets with a delay/duration
26
27 307 shorter than the time resolutions of the GIs would appear to be simultaneous between the ASIs and GIs.
28
29 308 Even in such cases, the implications of observed onsets are presumably different between the ASIs and
30
31 309 GIs.

32
33
34 310 The delay of GI-onsets from ASI-onsets has been assumed to be small, at less than ~ 1 min (e.g., *Liou*
35
36 311 2010), without direct comparison of GIs and ASIs. Pi2s have been classical substorm onset signatures
37
38 312 (e.g., *Rostoker et al.* 1980; *Olson* 1999; *Nosé et al.* 2012). GI-onsets have been observed ~ 1 min prior to
39
40 313 Pi2s (*Liou et al.* 2000). This correspondence may verify that the delays of GI-onsets from ASI-onsets are
41
42 314 small. However, the present study and *Ieda et al.* (2016) suggest that major Pi2s are not likely associated
43
44 315 with the Akasofu substorm onset, but rather with the poleward expansion later in the ASIs. Thus, the
45
46 316 correspondence of GI-onsets (i.e., poleward expansion) to Pi2s does not necessarily imply that the delays
47
48 317 of GI-onsets from ASI-onsets are small. Rather, it suggests that the substorm onsets in the GIs are
49
50 318 delayed with respect to the AIB in ASIs by more than that expected, depending on the duration of the
51
52 319 AIB.

320 **Causes of Differences Between Ground and Satellite Images**

321 Poleward expansion was observed in both ASIs and GIs. This sudden change appeared to be even more
322
323 322 evident in the GIs (Figures 6b and 7b) than in the ASIs (Figures 6a and 7a), indicating that the practical
324
325 323 sensitivity of the GIs is sufficient to identify poleward expansion. In contrast, the AIB was not evident
324
325 324 in the GIs, indicating that the sensitivity of GIs is considerably less than that of ASIs for identifying the
325
326 325 AIB.

1
2
3
4
5
6
7
8
9
10
11
12
13
14
15
16
17
18
19
20
21
22
23
24
25
26
27
28
29
30
31
32
33
34
35
36
37
38
39
40
41
42
43
44
45
46
47
48
49
50
51
52
53
54
55
56
57
58
59
60
61
62
63
64
65

326 These results suggest that the different responses between ASIs and GIs may depend on the latitudinal
327 thickness of the auroras. Our interpretation is that the brightness of the aurora is underemphasized when
328 the target is thinner than the spatial resolution of the camera. This underemphasis is attributed to the
329 averaging of an area that includes both the thin aurora and the adjacent dark region. The AIB is less
330 evident in GIs, presumably because it is thin in terms of the latitude range, particularly at the beginning,
331 compared with the spatial resolution of GIs. Thus, its brightness would be reduced significantly by
332 area-averaging. In contrast, the poleward expansion includes a thickening of the bright aurora; thus, its
333 brightness would be reduced at the beginning but would not be reduced after the expansion has reached
334 the spatial resolution of GIs. That is, the increase in brightness would be overemphasized in GIs when it
335 begins to detect poleward expansion (i.e., auroral breakup).

336 Another possibility is that these different responses in ASIs and GIs may be attributed to the difference
337 in wavelengths used to observe the auroras. The difference in wavelength did not result in significant
338 differences in the brightness of the poleward expansion. However, it may contribute to difference in
339 the brightness of the AIB. Both satellite (170 nm) and ground (557.7 nm) images are expected to be
340 sensitive to precipitating electrons in the keV range. Thus, the difference in wavelength likely did not
341 contribute significantly to the difference in observed auroras if the onset was dominated by keV-range
342 electrons. However, precipitating electrons may belong to other energy ranges for the AIB. In such cases,
343 the difference in wavelength may contribute to the different responses.

344 The AIB was not evident in the GIs in the present case; in other cases, the AIB may be sometimes
345 visible in GIs depending on the conditions of auroras and cameras. However, the wide brightening is not
346 explicitly included in identifications of substorm onset in GIs (e.g., *Frey et al.* 2004; *Liou* 2010), although
347 it is not explicitly excluded. Thus, the AIB has not been typically recognized in GIs thus far. The AIB
348 would be difficult to recognize as a substorm onset (i.e., sudden brightening) in GIs, not only because
349 its brightness is underemphasized, but also because the increase in brightness of the following poleward
350 expansion is overemphasized. With these assumptions, it may be sometimes possible to recognize a weak
351 brightening in GIs as belonging to the AIB a few minutes prior to the major brightening (i.e., poleward
352 expansion).

353 **Clarifications of Substorm Onset Definitions**

354 We have inferred that the traditionally identified onset brightening in satellite GIs does not necessarily
355 correspond to the Akasofu substorm onset. Instead, it tends to represent the poleward expansion that

1
2
3
4 follows a few minutes later (Figure 11). Below, we discuss the reason why this interpretation has not
5
6 been widely recognized.
7

8 **Confusion Regarding Two Different Localized Brightenings** 9

10 Substorm onsets in GIs are traditionally identified by a localized brightening, which is labeled as auroral
11
12 breakup (e.g., *Frey et al.* 2004; *Liou* 2010). Note that the two-stage development of the Akasofu model
13
14 has not been required in these identifications, presumably because of the limited sensitivity of GIs. In
15
16 contrast, this localized brightening in GIs is sometimes (e.g., *Frank et al.* 2001b; *Morioka et al.* 2014)
17
18 specifically labeled as the (Akasofu) IB instead.
19

20
21 This confusion arises likely because it is not often recognized that the AIB (*Akasofu* 1964) is elongated
22
23 along longitudes instead when considered on a time scale of a few minutes. This wide AIB may appear
24
25 as localized (\ll 1 MLT hour) at the very beginning (\sim 10 sec) in the ASIs (e.g., *Liang et al.* 2008) (Figure
26
27 11). However, this weak aurora at the very beginning can be marginally recognized only on detailed
28
29 inspection of ASIs; thus, it is expected to be barely detectable by GIs owing to the limited sensitivity
30
31 and time resolution.
32

33
34 Moreover, such localized brightenings expand quickly in longitude, and the resultant wide aurora,
35
36 sometimes including auroral beads, should be more evident than localized auroras. It is unlikely that the
37
38 localized aurora at the very beginning was observed without observing the following brighter wide aurora.
39
40 Thus, the observed localized brightening in GIs is unlikely to correspond to the localized brightening at
41
42 the very beginning of the AIB in ASIs, at least in most cases.
43

44
45 As discussed above, the localized first brightenings in ASIs and GIs are not likely to represent the same
46
47 phenomenon. This difference has not been often appreciated, likely also because both brightenings are
48
49 referred to as “localized”. The first brightening in the GIs appears to be localized in wide-area images
50
51 such as the 2128:07 UT panel of Figure 3, but the same brightening does not appear to be localized
52
53 in expanded images such as that in Figure 6b-5. Thus, the term “localized” has different implications
54
55 between ASIs and GIs (Figure 11) depending on the size of the displayed area.
56

57 **Confusion Regarding Expansion Onset and Expansion Phase Onset** 58

59
60 As discussed above, localized brightening in GIs is sometimes confused as corresponding to the Akasofu
61
62 substorm onset. The same confusion arises likely because “expansion phase onset” sounds like the start
63
64 of poleward expansion. One such example is a statement of (*McPherron* 2016): “The instant at which
65
the aurora begins to expand poleward is called the onset of the expansion phase of the auroral substorm

1
2
3
4
5 386 (*Akasofu* 1964).” . This recognition is inconsistent with *Akasofu* (1964), as explained below.
6
7 387 A substorm is traditionally divided into three phases: the growth phase, the expansion phase, and the
8
9 388 recovery phase. Substorm onsets refer to the beginning of the expansion phase (e.g., *Baumjohann and*
10
11 389 *Treumann* 2012). The term “substorm onset” may be confused with the start of the growth phase and
12
13 390 is often explicitly referred to as the “substorm expansion phase onset,” which is the beginning of the
14
15 391 expansion phase, as this term itself defines.
16
17 392 The expansion phase is defined in *Akasofu* (1964) to begin with Stage 1 (AIB, i.e., without poleward
18
19 393 expansion), followed by Stage 2 (poleward expansion) a few minutes later (Figure 1). Thus, confusingly,
20
21 394 there is no poleward expansion at the beginning of the expansion “phase” onset in the *Akasofu* substorm
22
23 395 model. That is, “the instant at which the aurora begins to expand poleward” does not correspond to the
24
25 396 expansion “phase” onset by definition.
26

27 397 **Initial Brightening or Poleward Expansion as a Substorm Onset**

28
29 398 The two-stage development in the original definition of substorm onset has not been emphasized in later
30
31 399 studies. For example, *Rostoker et al.* (1980) summarized various signatures to identify substorm onsets to
32
33 400 include auroral arc brightenings, negative bays, positive bays, and Pi2s. *Meng and Liou* (2004) identified
34
35 401 substorm onset as an auroral breakup, which they defined as a sudden brightening followed by poleward
36
37 402 expansion. Such studies did not discuss these signatures in the context of the two-stage development;
38
39 403 rather, they implicitly assumed only one unique instance can be identified as the substorm onset.
40
41 404 In contrast, different stages have been used to define substorm onsets in recent studies. The AIB (i.e.,
42
43 405 the original definition, Stage 1) is sometimes adopted to identify substorm onsets (e.g., *Donovan et al.*
44
45 406 2008). Poleward expansion (i.e., Stage 2) is instead adopted with (e.g., *Mende et al.* 2009) or without
46
47 407 (e.g., *McPherron* 2016) the recognition that this and the original definition differ. Substorm onsets in
48
49 408 GIs are usually identified by the sudden brightening (e.g., *Frey et al.* 2004; *Liou* 2010). In contrast,
50
51 409 *Morioka et al.* (2014) recognized in GIs that the sudden brightening is followed by another brightening a
52
53 410 few minutes later; they identified the substorm expansion phase onset by this second brightening in GIs.
54
55 411 As summarized above, the definition of a substorm onset (i.e., substorm expansion phase onset) is
56
57 412 currently diverging and is sometimes confused. To avoid such confusion, individual studies that include
58
59 413 discussions within a few minutes of accuracy are recommended to state the definition of substorm onsets
60
61 414 explicitly in the context of two-stage development. Two major possible definitions, AIB and poleward
62
63 415 expansion, are discussed below.
64
65

1
2
3
4 416 If the substorm onset is defined as the first signature, it is likely to correspond to AIB, which is the
5
6 417 original definition of onsets. Practically, this onset can be regularly monitored only by using ASIs. It
7
8 418 may include auroral rays or beads and is often too evident to ignore before the beginning of poleward
9
10 419 expansion. The AIB may be a manifestation of the triggering process of substorms, such as near-earth
11
12 420 instabilities or the initial stage of tail reconnection. Even the AIB may play an active role in triggering
13
14 421 substorms, for example, by feedback processes with the enhancement of ionospheric conductance and
15
16 422 current. However, it may also be possible that the AIB is not directly associated with substorm onsets
17
18 423 and occurs under background conditions favorable for the occurrence of substorm onsets.

19
20
21 424 In contrast, if the substorm onset is defined as the beginning of an explosive release of energy from the
22
23 425 tail to the polar ionosphere, it is likely to correspond to poleward expansion. The poleward expansion
24
25 426 presumably maps to dipolarization in the tail (e.g., *Chu et al.* 2015), thus manifesting the explosive
26
27 427 energy release. Because the dipolarization is a drastic change in the magnetic field lines, it would cause
28
29 428 major magnetic oscillations (i.e., major Pi2s). This onset can be identified by using various data sets
30
31 429 such as GIs and geomagnetic fields in addition to ASIs, and is thus useful at least as a working definition.
32
33 430 However, it should be remembered that poleward expansion is not the original definition (*Akasofu* 1964)
34
35 431 to time the substorm onsets.

36 37 38 432 **Impacts on Past Tail Reconnection Timing**

39
40 433 Reconnection-associated fast plasma flows are often observed in the magnetotail near the time of a
41
42 434 substorm onset identified by using Pi2s or GIs (*Hones et al.* 1984; *Moldwin and Hughes* 1993; *Slavin*
43
44 435 *et al.* 2002; *Ieda et al.* 2008). These fast flows have occasionally been further identified a few minutes
45
46 436 prior to the substorm onset (*Nagai et al.* 1998; *Ohtani et al.* 1999; *Baker et al.* 2002; *Kepko et al.* 2004;
47
48 437 *Miyashita et al.* 2009).

49
50
51 438 However, such conclusions depend on the definition of substorm onset. Whether the identified substorm
52
53 439 onset corresponds to the AIB or poleward expansion in ASIs has not been specified in these previous
54
55 440 studies. In the present study, the onsets in Pi2s and GIs corresponded to poleward expansion rather than
56
57 441 the Akasofu substorm onset. This result suggests that unless the longitudinally wide AIB was explicitly
58
59 442 considered, the substorm onsets identified in past studies did not correspond to the Akasofu substorm
60
61 443 onset but rather to poleward expansion.

62
63 444 Fast flows have always been initiated within a few minutes of the isolated auroral breakup in GIs
64
65 445 (i.e., poleward expansion) if the satellite was located near the onset-MLT (*Ieda et al.* 2008). However,

1
2
3
4 446 unobserved AIB may have occurred prior to the auroral breakup (i.e., poleward expansion). Thus, these
5
6 447 fast flows may be delayed from the possible AIB, as was reported in a case study by *Ieda et al.* (2016). In
7
8 448 summary, no evidence exists for reconnection-associated fast flows prior to the Akasofu substorm onset.
9
10 449 Therefore, the developed reconnection does not likely trigger the Akasofu substorm onset.
11
12 450 Reconnection-associated fast flows may be associated with auroral streamers. Some brightenings (e.g.,
13
14 451 2126:17 UT panel) occurred near 73 MLAT near the onset MLT sector in Figures 3a and 3b. Interestingly,
15
16 452 an auroral streamer was formed at 72 MLAT near the onset MLT simultaneously with the breakup
17
18 453 (2128:07 UT panel). This simultaneous occurrence may be a coincidence, or it may suggest that the
19
20 454 auroral breakup (i.e., poleward expansion) and tail reconnection occur simultaneously.
21
22
23
24

25 455 **Summary**

26
27 456 We have emphasized that the original definition of a substorm onset (Akasofu substorm onset) includes
28
29 457 two-stage development: the AIB, which is wide in longitude, followed by poleward expansion a few
30
31 458 minutes later. This two-stage development was originally proposed on the basis of ASIs. It has been
32
33 459 unclear thus far how this two-stage development is observed in satellite GIs, in which the time resolution
34
35 460 and sensitivity are limited.
36
37

38 461 In the present study, we directly compared optical substorm onset signatures observed in GIs and ASIs
39
40 462 for an event that occurred on December 7, 1999. We used ultraviolet GIs captured by the Polar satellite
41
42 463 during a fixed filter mode at 170 nm, enabling a high time resolution of 37 s to resolve the possible two-
43
44 464 stage development. The 20-s resolution green-line ASIs in Finland, at 557.7 nm, were used for comparison.
45
46 465 Our results and discussions are summarized as follows.
47

48
49 466 (1) A substorm onset was observed in the ASIs. These observations are consistent with the Akasofu
50
51 467 substorm model, as expected, because the two-stage development was evident: A longitudinally extended
52
53 468 brightening was followed by poleward expansion a few minutes later. In contrast, two-stage development
54
55 469 was not evident in the GIs, even with the high time resolution of 37 s in the present case. Instead, the
56
57 470 onset and poleward expansion occurred simultaneously in the GIs, as was the case in previous studies
58
59 471 with a practical time resolution of a few minutes.

60
61 472 (2) A comparison of ASIs and GIs revealed that poleward expansion occurred simultaneously, or within
62
63 473 1 min; however, the AIB in the ASIs did not have a counterpart in the GIs. Consequently, the substorm
64
65 474 onset identified by using GIs was delayed by 3 min from the onset identified by using ASIs. This result

1
2
3
4 suggests that the substorm onsets in GIs represent the beginning of poleward expansion rather than the
5
6 AIB.

7
8
9 (3) Major geomagnetic negative bays, positive bays, and mid-latitude Pi2 pulsations were observed within
10
11 1 min after the poleward expansion but 3–4 min after the Akasofu substorm onset. Thus, the classic
12
13 geomagnetic substorm signatures represent poleward expansion rather than the Akasofu substorm onset.
14
15 This result suggests that the substorm onsets identified in GIs and geomagnetic data correspond to the
16
17 same phenomenon (i.e., poleward expansion) but not to the Akasofu substorm onset.

18
19 (4) We discussed that substorm onsets identified in past studies do not necessarily correspond to the
20
21 Akasofu substorm onset but to subsequent poleward expansions, unless the AIB in ASIs was considered.
22
23 The AIB is underemphasized and the poleward expansion is overemphasized in GIs because of the limited
24
25 spatial resolution of GIs. Accordingly, poleward expansion tends to be identified as the substorm onset
26
27 in GIs even when the AIB is moderately visible in ASIs.

28
29 (5) Poleward expansion is useful as a working definition of substorm onset because the AIB is not regularly
30
31 monitored and can be gradual. It should be noticed that this definition using poleward expansion (i.e.,
32
33 Stage 2) is not the original definition (i.e., Stage 1) of substorm onset.

34
35 (6) We also discussed that the causality between tail reconnection and substorm onset depends on the
36
37 definition of substorm onset. In past studies, reconnection-associated fast flows have been observed
38
39 simultaneously or, in rare cases, prior to the substorm onset. However, because these onsets were identified
40
41 by Pi2s or GIs, they were likely to correspond to subsequent poleward expansion rather than Akasofu
42
43 substorm onsets. Thus, classical fast flows are associated with substorm onsets if the substorm onsets are
44
45 defined by poleward expansion, but may not be directly associated with substorm onsets if the substorm
46
47 onsets are defined by the AIB.

48 49 50 51 52 53 **Conclusion**

54
55 At least two different instances have been considered for substorm onset in previous studies: the AIB
56
57 (the original definition) and the poleward expansion (auroral breakup). It is necessary to clarify which
58
59 instance is selected to time the substorm onset to understand the time history of substorms, including
60
61 tail reconnection. For this purpose, we proposed a working model (Figure 11) to synthesize the three
62
63 different views of substorm onset: in the original Akasofu model, ASIs, and GIs. In the present study,
64
65 “GIs” specifically refer to images with a practical spatial resolution of ~ 50 km or slightly worse, such as

1
2
3
4
5 504 Polar/UVI or IMAGE/FUV images.

6
7 505 We suggest that substorm onset identified by GIs represents poleward expansion rather than the AIB.

8
9 506 Although the AIB may be visible, its identification as a substorm onset would be less convincing in GIs.

10
11 507 The two-stage development is not evident in GIs because their spatial resolution is limited. The practical

12
13 508 significance of these inferences depends on the duration and intensity of the AIB, which is currently not

14
15 509 well established.

16 17 18 19 510 **List of abbreviations**

20
21 511 AIB: Akasofu initial brightening; ASI: ground-based all-sky image; CCD: charged couple device; FUV: far

22
23 512 ultraviolet imager onboard the IMAGE satellite; GI: satellite-based global image; IMAGE project: Inter-

24
25 513 national Monitor for Auroral Geomagnetic Effects project; IMAGE satellite: Imager for Magnetopause-

26
27 514 to-Aurora Global Exploration satellite; IB: initial brightening; LBHL: Lyman-Birge-Hopfield long; LBHS:

28
29 515 Lyman-Birge-Hopfield short; MLAT: magnetic latitude in degrees; MLON: magnetic longitude in degrees;

30
31 516 MLT: magnetic local time in hours; MUO: Muonio in Finland; OMNI: Operating Missions as Nodes on

32
33 517 the Internet; SAMNET: Sub-Auroral Magnetometer Network project; UVI: ultraviolet imager onboard

34
35 518 the Polar satellite.

36 37 38 39 40 519 **Competing interests**

41
42 520 The authors declare that they have no competing interests.

43 44 45 46 521 **Authors' contributions**

47
48 522 AI performed the data analysis and drafted the manuscript. KK and DW contributed to the data

49
50 523 analysis of all-sky images. YN, YM, HUF, MN, YM, TM, TK, and SM helped to interpret the data.

51
52 524 MOF contributed to data analysis of the satellite images. LJ contributed to the data analysis of IMAGE

53
54 525 geomagnetic field. FH and NCR contributed to data analysis of the SAMNET geomagnetic field. All

55
56 526 authors approved the final manuscript.

57 58 59 60 61 527 **Acknowledgments**

62
63 528 A.I. thanks S.-I. Akasofu, D. H. Fairfield, K. Kamide, A. Ketola, M. Kubota, K. Liou, D.

64
65 529 Lummerzheim, T. Nagai, A. Nishida, N. Partamies, and H. Vanhamäki for their valuable comments.

1
2
3
4 530 F.H. acknowledges fruitful discussions of the results from this research with colleagues at the
5
6 531 International Space Science Institute, Bern, Switzerland.
7
8 532 The authors acknowledge G. K. Parks for use of data from the Polar satellite ultraviolet imager
9
10 533 (<https://cdaweb.sci.gsfc.nasa.gov>).
11
12 534 The ground-based all-sky imager at Muonio and International Monitor for Auroral Geomagnetic Effects
13
14 535 (IMAGE) magnetometers are a part of the Magnetometers-Ionospheric Radars-All-sky Cameras Large
15
16 536 Experiment (MIRACLE, <http://space.fmi.fi/MIRACLE/>), under the leadership of the Finnish
17
18 537 Meteorological Institute. The authors thank the institutes that maintain the IMAGE magnetometer
19
20
21 538 array.
22
23 539 The Sub-Auroral Magnetometer Network data (SAMNET) is operated by the Space and Planetary
24
25 540 Physics Group, Department of Physics, Lancaster University. Data obtained from the SAMNET project
26
27 541 (<http://spears.lancs.ac.uk/samnet/>) include data (Lerwick, Hartland and Eskdalemuir) courtesy of the
28
29 542 British Geological Survey, and IMAGE stations data (Hankasalmi, Oulujärvi, Uppsala) courtesy of the
30
31 543 Finnish Meteorological Institute, University of Oulu, and the Geological Survey of Sweden.
32
33 544 The OMNI data were obtained from the GSFC/SPDF OMNIWeb interface at
34
35 545 <https://omniweb.gsfc.nasa.gov>. The AL, AU, and SYM-H indices were derived by the WDC for
36
37 546 Geomagnetism, Kyoto. The Kp index was derived by the GFZ Potsdam, Germany. The code of the
38
39 547 modified magnetic apex coordinates was received from the CEDAR database at NCAR, which is
40
41 548 supported by NSF.
42
43 549 This work was supported by JSPS KAKENHI grants 16K05568, 26247082, 16H04057, and 26610143.
44
45 550 This work was also supported by NASA NNX15AI62G, NSF AGS-1451911, and AFOSR
46
47 551 FA9550-15-1-0179.
48
49
50
51
52

552 **References**

- 553 Akasofu, S.-I. (1963), Dynamical morphology of aurora polaris, *J. Geophys. Res.*, *68*(6), 1667–1673,
554 doi:10.1029/JZ068i006p01667.
555 Akasofu, S.-I. (1964), The development of the auroral substorm, *Planet. Space Sci.*, *12*(4), 273–282,
556 doi:10.1016/0032-0633(64)90151-5.
557 Akasofu, S.-I. (1977), *Physics of magnetospheric substorms*, D. Reidel Publishing Company, Dordrecht,
558 Holland.

1
2
3
4
5
6
7
8
9
10
11
12
13
14
15
16
17
18
19
20
21
22
23
24
25
26
27
28
29
30
31
32
33
34
35
36
37
38
39
40
41
42
43
44
45
46
47
48
49
50
51
52
53
54
55
56
57
58
59
60
61
62
63
64
65

559 Akasofu, S.-I. (2012), Auroral morphology: A historical account and major auroral features during
560 auroral substorms, in *Auroral Phenomenology and Magnetospheric Processes: Earth and Other*
561 *Planets*, vol. 197, edited by A. Keiling, E. Donovan, F. Bagenal, and T. Karlsson, pp. 29–38,
562 doi:10.1029/2011gm001156.

563 Akasofu, S. I., A. T. Y. Lui, and C. I. Meng (2010), Importance of auroral features in the search for
564 substorm onset processes, *J. Geophys. Res.*, *115*, doi:10.1029/2009ja014960.

565 Baker, D. N., et al. (2002), Timing of magnetic reconnection initiation during a global magnetospheric
566 substorm onset, *Geophys. Res. Lett.*, *29*(24), doi:10.1029/2002gl015539.

567 Baumjohann, W., and R. A. Treumann (2012), *Basic space plasma physics*, revised ed., Imperial
568 College Press, London.

569 Bristow, W. A., et al. (2003), Detailed analysis of substorm observations using SuperDARN, UVI,
570 ground-based magnetometers, and all-sky imagers, *J. Geophys. Res.*, *108*(A3),
571 doi:10.1029/2002ja009242.

572 Chu, X., et al. (2015), Magnetic mapping effects of substorm currents leading to auroral poleward
573 expansion and equatorward retreat, *J. Geophys. Res.*, *120*(1), 253–265, doi:10.1002/2014ja020596.

574 Donovan, E., et al. (2006), The azimuthal evolution of the substorm expansive phase onset aurora, in
575 *Proceedings of Eighth International Conference on Substorms (ICS-8)*, edited by M. Syrjäsuo and
576 E. Donovan, pp. 55–60, University of Calgary, Calgary, Alberta, Canada.

577 Donovan, E., et al. (2008), Simultaneous THEMIS in situ and auroral observations of a small substorm,
578 *Geophys. Res. Lett.*, *35*(17), doi:10.1029/2008gl033794.

579 Elvey, C. T. (1957), Problems of auroral morphology, *Proceedings of the National Academy of Sciences*
580 *of the United States of America*, *43*(1), 63–75, doi:10.1073/pnas.43.1.63.

581 Frank, L. A., J. B. Sigwarth, W. R. Paterson, and S. Kokubun (2001a), Two encounters of the
582 substorm onset region with the Geotail spacecraft, *J. Geophys. Res.*, *106*(A4), 5811–5831,
583 doi:10.1029/2000ja003040.

584 Frank, L. A., W. R. Paterson, J. B. Sigwarth, and T. Mukai (2001b), Observations of plasma sheet
585 dynamics earthward of the onset region with the Geotail spacecraft, *J. Geophys. Res.*, *106*(A9),
586 18,823–18,841, doi:10.1029/2000ja000419.

587 Frey, H. U., and S. B. Mende (2006), Substorm onsets as observed by IMAGE-FUV, in *Proceedings of*
588 *Eighth International Conference on Substorms (ICS-8)*, edited by M. Syrjäsuo and E. Donovan, pp.

- 1
2
3
4
589 71–75, University of Calgary, Calgary, Alberta, Canada.
- 590 Frey, H. U., S. B. Mende, V. Angelopoulos, and E. F. Donovan (2004), Substorm onset observations by
591 IMAGE-FUV, *J. Geophys. Res.*, *109*(A10), doi:10.1029/2004ja010607.
- 592 Frey, H. U., et al. (2010), Small and meso-scale properties of a substorm onset auroral arc, *J. Geophys.*
593 *Res.*, *115*, doi:10.1029/2010ja015537.
- 594 Galand, M., and D. Lummerzheim (2004), Contribution of proton precipitation to space-based auroral
595 FUV observations, *J. Geophys. Res.*, *109*(A3), doi:10.1029/2003ja010321.
- 596 Germany, G. A., et al. (1998), Auroral observations from the Polar ultraviolet imager (UVI), in
597 *Geospace Mass and Energy Flow: Results From the International Solar-Terrestrial Physics Program*,
598 vol. 104, edited by J. L. Horwitz, D. L. Gallagher, and W. K. Peterson, pp. 149–160, American
599 Geophysical Union, Washington, DC.
- 600 Hones, E. W., et al. (1984), Structure of the magnetotail at 220-Re and its response to geomagnetic
601 activity, *Geophys. Res. Lett.*, *11*(1), 5–7, doi:10.1029/GL011i001p00005.
- 602 Ieda, A., et al. (2008), Longitudinal association between magnetotail reconnection and auroral breakup
603 based on Geotail and Polar observations, *J. Geophys. Res.*, *113*(A8), doi:10.1029/2008ja013127.
- 604 Ieda, A., et al. (2016), Stepwise tailward retreat of magnetic reconnection: THEMIS observations of an
605 auroral substorm, *J. Geophys. Res.*, *121*(5), 4548–4568, doi:10.1002/2015ja022244.
- 606 Juusola, L., K. Kauristie, H. Vanhamäki, A. Aikio, and M. van de Kamp (2016), Comparison of auroral
607 ionospheric and field-aligned currents derived from Swarm and ground magnetic field measurements,
608 *J. Geophys. Res.*, *121*(9), 9256–9283, doi:10.1002/2016ja022961.
- 609 Kepko, L., M. G. Kivelson, R. L. McPherron, and H. E. Spence (2004), Relative timing of substorm
610 onset phenomena, *J. Geophys. Res.*, *109*(A4), doi:10.1029/2003ja010285.
- 611 King, J. H., and N. E. Papitashvili (2005), Solar wind spatial scales in and comparisons of hourly Wind
612 and ACE plasma and magnetic field data, *J. Geophys. Res.*, *110*(A2), doi:10.1029/2004ja010649.
- 613 Liang, J., et al. (2008), Intensification of preexisting auroral arc at substorm expansion phase onset:
614 Wave-like disruption during the first tens of seconds, *Geophys. Res. Lett.*, *35*(17),
615 doi:10.1029/2008gl033666.
- 616 Liou, K. (2010), Polar Ultraviolet Imager observation of auroral breakup, *J. Geophys. Res.*, *115*,
617 doi:10.1029/2010ja015578.
- 618 Liou, K., et al. (1999), On relative timing in substorm onset signatures, *J. Geophys. Res.*, *104*(A10),

- 1
2
3
4
5 619 22,807–22,817, doi:10.1029/1999ja900206.
- 6
7 620 Liou, K., et al. (2000), Evaluation of low-latitude Pi2 pulsations as indicators of substorm onset using
8
9 621 Polar ultraviolet imagery, *J. Geophys. Res.*, *105*(A2), 2495–2505, doi:10.1029/1999ja900416.
- 10
11 622 Lummerzheim, D., et al. (1997), High time resolution study of the hemispheric power carried by
12
13 623 energetic electrons into the ionosphere during the May 19/20, 1996 auroral activity, *Geophys. Res.*
14
15 624 *Lett.*, *24*(8), 987–990, doi:10.1029/96gl03828.
- 16
17 625 Lyons, L. R., Y. Nishimura, E. Donovan, and V. Angelopoulos (2013), Distinction between auroral
18
19 626 substorm onset and traditional ground magnetic onset signatures, *J. Geophys. Res.*, *118*(7),
20
21 627 4080–4092, doi:10.1002/jgra.50384.
- 22
23 628 McPherron, R. L. (2016), Where and when does reconnection occur in the tail?, *J. Geophys. Res.*,
24
25 629 *121*(5), 4607–4610, doi:10.1002/2015ja022258.
- 26
27 630 Mende, S., et al. (2009), Timing and location of substorm onsets from THEMIS satellite and ground
28
29 631 based observations, *Ann. Geophys.*, *27*(7), 2813–2830, doi:10.5194/angeo-27-2813-2009.
- 30
31 632 Meng, C. I., and K. Liou (2004), Substorm timings and timescales: A new aspect, *Space Sci. Rev.*,
32
33 633 *113*(1-2), 41–75, doi:10.1023/b:spac.0000042939.88548.68.
- 34
35 634 Miyashita, Y., et al. (2009), A state-of-the-art picture of substorm-associated evolution of the
36
37 635 near-Earth magnetotail obtained from superposed epoch analysis, *J. Geophys. Res.*, *114*,
38
39 636 doi:10.1029/2008ja013225.
- 40
41 637 Moldwin, M. B., and W. J. Hughes (1993), Geomagnetic substorm association of plasmoids, *J. Geophys.*
42
43 638 *Res.*, *98*(A1), 81–88, doi:10.1029/92ja02153.
- 44
45 639 Morioka, A., et al. (2014), Substorm onset process: Ignition of auroral acceleration and related
46
47 640 substorm phases, *J. Geophys. Res.*, *119*(2), 1044–1059, doi:10.1002/2013ja019442.
- 48
49 641 Motoba, T., S. Ohtani, A. Kadokura, and J. Gjerloev (2014), Interrelationship between preonset auroral
50
51 642 and magnetic signatures at a geomagnetically conjugate Iceland-Syowa pair, *J. Geophys. Res.*,
52
53 643 *119*(2), 761–769, doi:10.1002/2013ja019512.
- 54
55 644 Nagai, T., et al. (1998), Structure and dynamics of magnetic reconnection for substorm onsets with
56
57 645 Geotail observations, *J. Geophys. Res.*, *103*(A3), 4419–4440, doi:10.1029/97ja02190.
- 58
59 646 Nishimura, Y., et al. (2012), Formation of substorm Pi2: A coherent response to auroral streamers and
60
61 647 currents, *J. Geophys. Res.*, *117*, doi:10.1029/2012ja017889.
- 62
63
64
65 648 Nishimura, Y., et al. (2016), Statistical properties of substorm auroral onset beads/rays, *J. Geophys.*

1
2
3
4
5 649 *Res.*, 121(9), 8661–8676, doi:10.1002/2016ja022801.
6
7 650 Nosé, M., et al. (2012), Wp index: A new substorm index derived from high-resolution geomagnetic
8
9 651 field data at low latitude, *Space Weather*, 10, doi:10.1029/2012sw000785.
10
11 652 Ohtani, S., et al. (1999), Substorm onset timing: The December 31, 1995, event, *J. Geophys. Res.*,
12
13 653 104(A10), 22,713–22,727, doi:10.1029/1999ja900209.
14
15 654 Olson, J. V. (1999), Pi2 pulsations and substorm onsets: A review, *J. Geophys. Res.*, 104(A8),
16
17 655 17,499–17,520, doi:10.1029/1999ja900086.
18
19 656 Partamies, N., L. Juusola, D. Whiter, and K. Kauristie (2015), Substorm evolution of auroral
20
21 657 structures, *J. Geophys. Res.*, 120(7), 5958–5972, doi:10.1002/2015ja021217.
22
23 658 Rae, I. J., et al. (2009), Near-Earth initiation of a terrestrial substorm, *J. Geophys. Res.*, 114,
24
25 659 doi:10.1029/2008ja013771.
26
27 660 Richmond, A. D. (1995), Ionospheric electrodynamics using magnetic apex coordinates, *J. Geomag.*
28
29 661 *Geoelectr.*, 47(2), 191–212, doi:10.5636/jgg.47.191.
30
31 662 Rostoker, G., et al. (1980), Magnetospheric substorms - Definition and signatures, *J. Geophys. Res.*,
32
33 663 85(NA4), 1663–1668, doi:10.1029/JA085iA04p01663.
34
35 664 Sangalli, L., et al. (2011), Performance study of the new EMCCD-based all-sky cameras for auroral
36
37 665 imaging, *International Journal of Remote Sensing*, 32(11), 2987–3003,
38
39 666 doi:10.1080/01431161.2010.541505.
40
41 667 Shiokawa, K., et al. (2005), Ground and satellite observations of substorm onset arcs, *J. Geophys. Res.*,
42
43 668 110(A12), doi:10.1029/2005ja011281.
44
45 669 Slavin, J. A., et al. (2002), Simultaneous observations of earthward flow bursts and plasmoid ejection
46
47 670 during magnetospheric substorms, *J. Geophys. Res.*, 107(A7), doi:10.1029/2000ja003501.
48
49 671 Syrjäsuo, M. T., et al. (1998), Observations of substorm electrodynamics using the MIRACLE network,
50
51 672 in *Substorms-4*, edited by S. Kokubun and Y. Kamide, pp. 111–114, Terra Scientific Publishing
52
53 673 Company / Kluwer Academic Publishers.
54
55 674 Tagirov, V. R., et al. (1998), Comparison of two substorm onsets on the basis of coordinated
56
57 675 ground-satellite observations, in *Substorms-4*, edited by S. Kokubun and Y. Kamide, pp. 339–342,
58
59 676 Terra Scientific Publishing Company / Kluwer Academic Publishers.
60
61 677 Tanskanen, E. I. (2009), A comprehensive high-throughput analysis of substorms observed by IMAGE
62
63 678 magnetometer network: Years 1993-2003 examined, *J. Geophys. Res.*, 114, doi:10.1029/2008ja013682.
64
65

1
2
3
4
5 679 Thebault, E., et al. (2015), International Geomagnetic Reference Field: the 12th generation, *Earth*
6
7 680 *Planets Space*, 67, doi:10.1186/s40623-015-0228-9.
8
9 681 Torr, M. R., et al. (1995), A far-ultraviolet imager for the international solar-terrestrial physics mission,
10
11 682 *Space Sci. Rev.*, 71(1-4), 329–383, doi:10.1007/bf00751335.
12
13 683 van de Kamp, M. (2013), Harmonic quiet-day curves as magnetometer baselines for ionospheric current
14
15 684 analyses, *Geoscientific Instrumentation Methods and Data Systems*, 2(2), 289–304,
16
17 685 doi:10.5194/gi-2-289-2013.
18
19 686 Viljanen, A., K. Kauristie, and K. Pajunpaa (1995), On induction effects at eiscat and image
20
21 687 magnetometer stations, *Geophys. J. Int.*, 121(3), 893–906, doi:10.1111/j.1365-246X.1995.tb06446.x.
22
23 688 Yago, K., et al. (2007), Simultaneous DMSP, all-sky camera, and IMAGE FUV observations of the
24
25 689 brightening are at a substorm pseudo-breakup, *Earth Planets Space*, 59(1), 45–49,
26
27 690 doi:10.1186/bf03352021.
28
29 691 Yeoman, T. K., D. K. Milling, and D. Orr (1990), Pi2 pulsation polarization patterns on the U.K.
30
31 692 subauroral magnetometer network (SAMNET), *Planet. Space Sci.*, 38(5), 589–602,
32
33 693 doi:10.1016/0032-0633(90)90065-x.
34
35 694 Zou, S., et al. (2010), Identification of substorm onset location and preonset sequence using Reimei,
36
37 695 THEMIS GBO, PFISR, and Geotail, *J. Geophys. Res.*, 115, doi:10.1029/2010ja015520.
38
39
40
41

696 **Figure Captions**

697 **Figure 1**

698 Original illustrations and figure captions of the Akasofu substorm onset (*Akasofu* 1964). Clarifications
699 are added on the top and bottom of the figure. The illustrated time sequence was proposed on the basis
700 of 1-min resolution ground all-sky images (ASIs). Auroral emissions in the polar ionosphere above 60°
701 magnetic latitude are illustrated. T = 0 min represents the time of the Akasofu substorm onset. (0) T
702 < 0: Quiet time. Quiet-time auroral arcs are shown. (1) T = 0–5 min: Akasofu initial brightening
703 (AIB; i.e., Akasofu substorm onset), starting at T = 0. Also called Stage 1 of the substorm expansion
704 phase. This brightening is wide in longitude without poleward expansion. (2) T = 5–10 min: Poleward
705 expansion, starting at T = 5. Also called Stage 2 of the substorm expansion phase. The two-stage
706 development has also been illustrated in later studies (e.g., *Akasofu et al.* 2010) and is essential in this
707 Akasofu substorm onset.

1
2
3
4
5 **Figure 2**

6
7
8
9
10
11
12
13
14
15
16
17
18
19
20
21
22
23
24
25
26
27
28
29
30
31
32
33
34
35
36
37
38
39
40
41
42
43
44
45
46
47
48
49
50
51
52
53
54
55
56
57
58
59
60
61
62
63
64
65

708 **Figure 2**
709 Example of simultaneous satellite-based global images and ground-based all-sky images (ASIs). These
710 images were observed at 2129 UT on December 7, 1999. (a1) Polar satellite global image in the raw
711 (CCD) coordinates with an overlaid geographical map. Auroral emission at ultraviolet 170 nm (LBHL)
712 is shown. (a2) The same satellite image as (a1) but in the magnetic coordinates (i.e., the modified
713 APEX coordinates). (b1) Ground-based all-sky image observed at Muonio (MUO, 64.6 MLAT, 105.2
714 MLON, 68.02°N, 23.53°E) in Lapland, Finland in the raw (CCD) coordinates. Auroral emission at
715 557.7 nm (green-line) is shown. (b2) The same ground image as (b1) but in the geodetic coordinates
716 (the azimuthal equidistant projection), trimmed at the elevation angle of 5°. The dashed white lines
717 indicate MLT and MLAT reference lines. The red line indicates the substorm onset MLT (23.2 h), from
718 where auroral keograms were made later. The red circles in (a1) and (b2) indicate the field-of-view of
719 the ASIs for the elevation angle of 10°, corresponding to a diameter of ~ 1000 km (~ 9° along
720 latitudes) to the assumed emission altitude of 110 km.

721 **Figure 3**

722 Polar satellite ultraviolet observations of an auroral breakup on December 7, 1999. Auroral brightness
723 at a wavelength of 170 nm (LBHL) is shown after projection in the modified APEX magnetic
724 coordinates at an altitude of 110 km in the polar ionosphere. The auroral brightness is converted to the
725 corresponding energy flux of precipitating electrons that cause auroras. (a) Time series of full-time
726 (36.8-s) resolution images shown in false color from left to right. The time labels of images were chosen
727 as the center of the image accumulation period (36.8 s for the present case). An auroral breakup (red
728 circle, 23.2 MLT, 64.6° MLAT) is first seen in the panel labeled 2128:07 UT in red. Because the
729 previous image was taken at 2127:30 UT, we estimate that the breakup began at 2127:49 UT (i.e., the
730 center time of the two images). (b) Auroral keogram sliced along the onset meridian (23.2 MLT, ± 0.2
731 h average). (c) Auroral brightness averaged over 23.0–23.4 MLT and 62–70 MLAT. The solid red line in
732 (b) and (c) indicates the breakup at 2127:49 UT. The dashed red line indicates 2124:50 UT.

733 **Figure 4**

734 Ground-based all-sky images (ASIs) near the substorm onset location on December 7, 1999. Auroral
735 brightness at a wavelength of 557.7 nm (green-line) observed at Muonio (MUO) in Finland is shown.
736 Time sequence of full-time-resolution (20-s) images from top to bottom in MLON–MLAT coordinates
737 between 64 and 65 MLAT. The red circle indicates the location of MUO. The red line indicates 23.2

1
2
3
4 738 MLT, the approximate location of the initiation of the Akasofu initial brightening (AIB) and the
5
6 739 poleward expansion.

7
8 **Figure 5**
9

10 741 Ground-based all-sky images (ASIs) near the substorm onset location on December 7, 1999. Auroral
11
12 742 brightness at a wavelength of 557.7 nm (green-line) observed at Muonio (MUO) in Finland is shown.
13
14
15 743 (a) Selected images that represent three intervals as labeled, shown in the geodetic coordinates. The
16
17 744 white reference lines represent MLTs and MLATs. The red line indicates 23.2 MLT, the approximate
18
19 745 location of the initiation of the Akasofu initial brightening (AIB) and the poleward expansion. (b)
20
21 746 Auroral keograms sliced along the onset meridian (23.2 MLT, ± 0.2 h average), which correspond to the
22
23 747 red lines in (a). (c) Time series of auroral brightness near the onset location (23.2 MLT, 64.6 MLAT),
24
25 748 averaged over 23.0–23.4 MLT and 64.5–64.7 MLAT. The red vertical lines in (b) and (c) indicate the
26
27 749 times of the AIB (2124:50 UT) and the poleward expansion (2127:50 UT) in the ASIs.

28
29 **Figure 6**
30

31
32 751 Comparison of (a) ground-based and (b) satellite-based auroral images on December 7, 1999. The time
33
34 752 sequence of selected auroral images is shown from top to bottom. All images are projected to the same
35
36 753 area in geodetic coordinates. (a) Ground-based all-sky images (ASIs; 557.7 nm) at the Muonio station
37
38 754 (MUO) in Finland. These ASIs were selected to show the observed instances (a1) during the quiet
39
40 755 interval, (a2) at the start of Akasofu initial brightening (AIB), (a3)–(a4) during AIB, (a5) at the start
41
42 756 of poleward expansion, and (a6) during poleward expansion. (b) Global images (170 nm) taken by the
43
44 757 Polar satellite ultraviolet imager (UVI). Each image was selected to form a pair with an ASI in (a)
45
46 758 within 7 s. A comparison of (a) and (b) reveals that the longitudinally extended brightening (AIB) can
47
48 759 be marginally observed in (a2) and is evident in (a3)–(a4) but not in (b2)–(b4). In contrast, the
49
50 760 brightening (a5) that corresponds to the beginning of the poleward expansion was simultaneously
51
52 761 observed in (b5).

53
54 **Figure 7**
55

56
57 763 Comparison of (a) ground-based and (b) satellite-based observations of auroras on December 7, 1999.
58
59 764 The time series of full-time-resolution images were sliced along the onset meridian (23.2 MLT, ± 0.2 h
60
61 765 average) and are shown as auroral keograms. The red vertical lines indicate the times of the Akasofu
62
63 766 initial brightening (AIB) and the poleward expansion, which were identified in the original
64
65 767 ground-based images. The poleward expansion (i.e., auroral breakup) at 2127:50 UT was

1
2
3
4 768 simultaneously observed in both ASIs and GIs. The AIB was observed at 2124:50 UT in the ASIs but
5
6 769 was not evident in the GIs against noise-level fluctuations.

7
8
9 770 **Figure 8**

10 771 Solar wind parameters and geomagnetic indices on December 7, 1999. These data were obtained from
11
12 772 the Operating Missions as Nodes on the Internet (OMNI) data set. The red vertical lines indicate the
13
14 773 Akasofu initial brightening (AIB; 2124:50 UT) and the poleward expansion (2127:50 UT) identified by
15
16 774 using all-sky images (ASIs). The solar wind parameters were time-shifted with respect to the bow shock
17
18 775 nose. Geocentric solar magnetospheric (GSM) coordinates were used. The interplanetary magnetic field
19
20 776 (IMF) was weakly southward ($B_z \sim -1$ nT) and strongly duskward ($B_y \sim 6$ nT), indicating
21
22 777 moderately favorable conditions for the occurrence of substorms. The AL index (i.e., westward
23
24 778 ionospheric current) began to develop at 2129 UT, which is closer in time to the poleward expansion
25
26 779 than to the AIB in the ASIs.

27
28
29 780 **Figure 9**

30 781 IMAGE ground magnetic observations near the substorm onset longitude in Europe. (a) Variations in
31
32 782 the northward (X), eastward (Y), and downward (Z) components of the magnetic field in geomagnetic
33
34 783 coordinates. The panels are presented in order of the observatory latitude, with the top panel
35
36 784 corresponding to the highest magnetic latitude (MLAT) station. The magnetic local time (MLT) of
37
38 785 each observatory at 2127 UT is shown at the left of each panel. Red vertical lines indicate the times of
39
40 786 the Akasofu initial brightening (AIB) at 2124:50 UT and the poleward expansion at 2127:50 UT, both
41
42 787 at [23.2 MLT, 64.6 MLAT] in the all-sky images (ASIs). The five-quiet-day baseline was subtracted for
43
44 788 each observatory. The negative bay began at 2128 UT. (b) Intensity of the equivalent current at an
45
46 789 altitude of 110 km, shown along the KIR station meridian (103° magnetic longitude). The equivalent
47
48 790 current was derived by using the same data set as (a), except that the *van de Kamp* (2013) baseline was
49
50 791 used. (c) Expansion of (a) for weak variations beginning at 2124 UT. The average of the displayed
51
52 792 interval was subtracted for each observatory. (d) Locations of some IMAGE magnetic stations overlaid
53
54 793 on an ASI at Muonio captured during the AIB.

55
56
57 794 **Figure 10**

58
59 795 SAMNET ground magnetic observations near the substorm onset longitude below 60 MLAT. The
60
61 796 format is the same as that of the IMAGE magnetic observations in Figure 9a, except that the 1-s values
62
63 797 are shown and the average of the displayed interval was subtracted for each observatory. Pi2 and
64
65

1
2
3
4
5 798 positive bay began at 2128:50 UT.

6
7 799 **Figure 11**

8
9 800 Synthesis of three different views of auroral substorm onset observations: (a) original concept (*Akasofu*
10 801 1964) based on 1-min resolution ground-based all-sky images (ASIs); (b) high time resolution ($< \sim 10$ s)
11
12 802 ASIs; (c) satellite-based global images (resolution of a few minutes). The spatial resolution of ASIs
13
14 803 (~ 1 km) is much better than that of global images (~ 50 km). From top to bottom, the time sequence
15
16 804 of auroral emissions on the nightside ionosphere above 60° magnetic latitude is illustrated. The blue,
17
18 805 green, and red colors indicate weak, moderate, and intense recorded auroral emissions, respectively. The
19
20 806 initial brightening (IB) is longitudinally extended, shown as Akasofu IB (AIB) in (a). This AIB may
21
22 807 appear as localized at the beginning followed by rapid longitudinal expansion (auroral rays or auroral
23
24 808 beads) in (b), as indicated by green circles. Red circles indicate poleward expansion (i.e., auroral
25
26 809 breakup). A substorm onset is identified by the AIB in (a), and practically by the poleward expansion
27
28 810 in (c). It is undecided whether the localized IB or the poleward expansion should be used to define the
29
30 811 substorm onset in (b). Auroral brightness is significantly underemphasized in global images, presumably
31
32 812 by area-averaging when the aurora is latitudinally thinner than the spatial resolution of the images.
33
34
35
36
37
38
39
40
41
42
43
44
45
46
47
48
49
50
51
52
53
54
55
56
57
58
59
60
61
62
63
64
65

Original substorm onset

Akasofu 1964; 2010

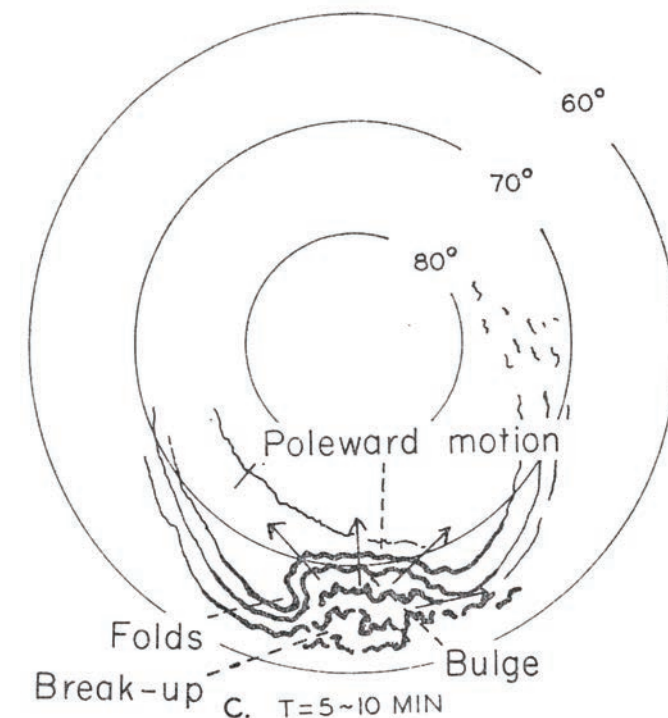
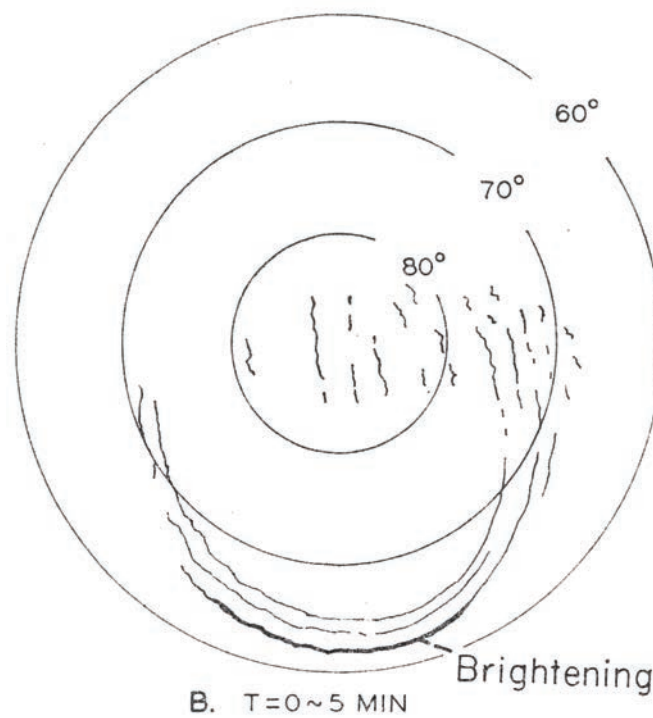
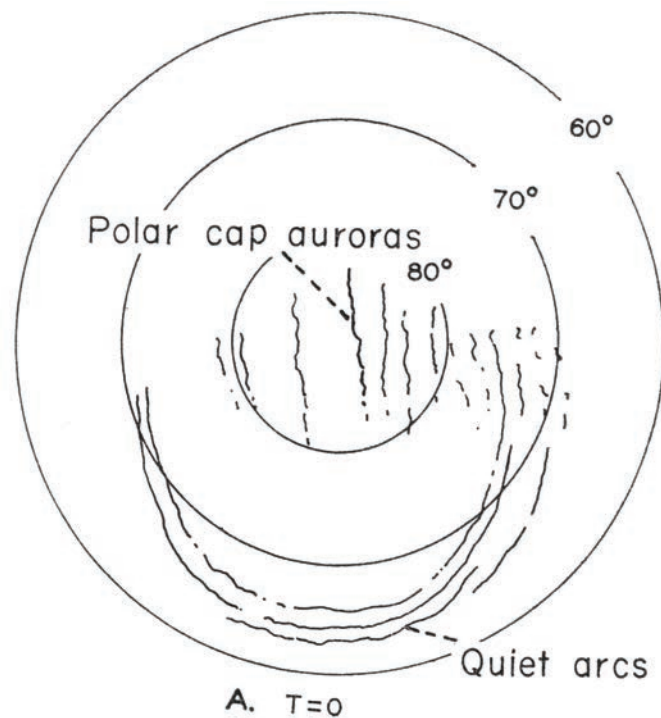


FIG. 2. THE DISTRIBUTION OF THE AURORAS DURING THE QUIET PHASE.

FIG. 3. AURORAS DURING THE EXPANSIVE PHASE (STAGE I).

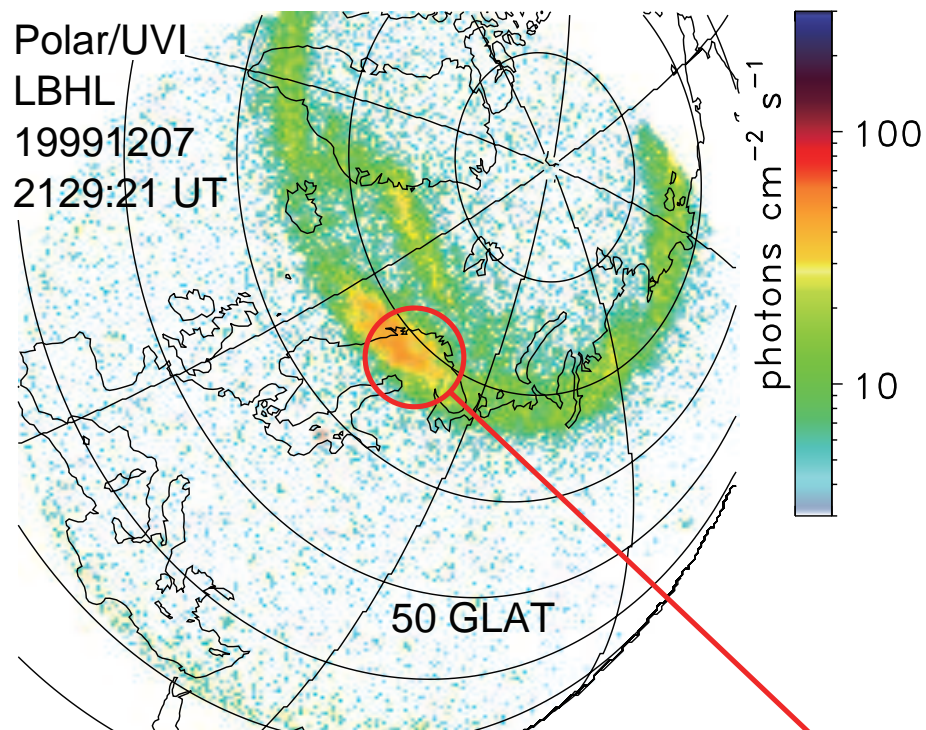
FIG. 4. AURORAS DURING THE EXPANSIVE PHASE (STAGE II).

(0) Time < 0:
Quiet phase:
Quiet arc

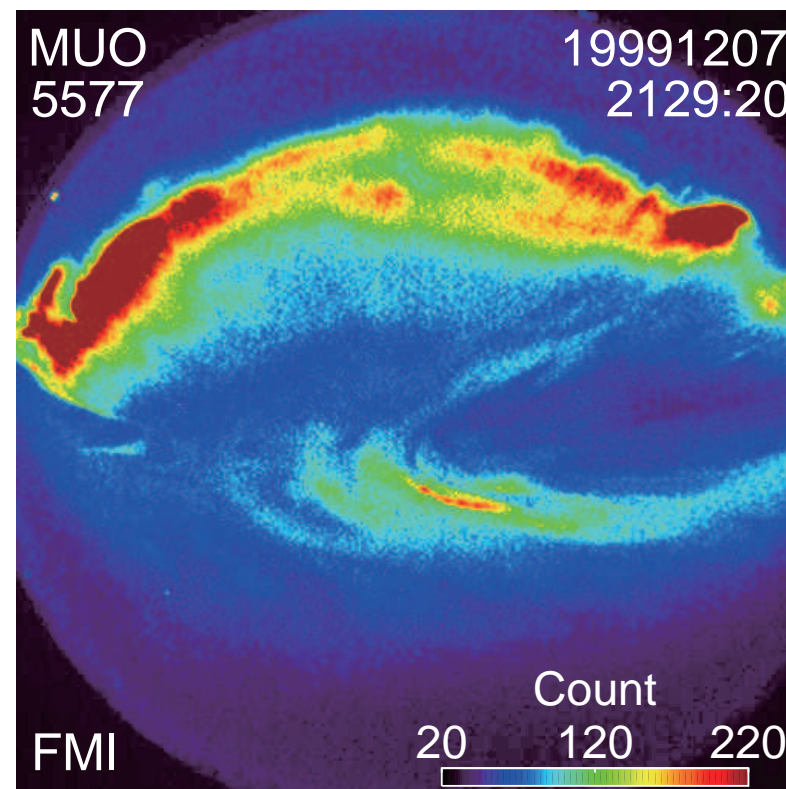
(1) $T=0-5 \text{ min}$:
EXP-phase Stage 1:
Initial brightening
(Akasofu onset)

(2) $T=5-10 \text{ min}$:
EXP-phase Stage 2:
Poleward expansion
(Auroral breakup)

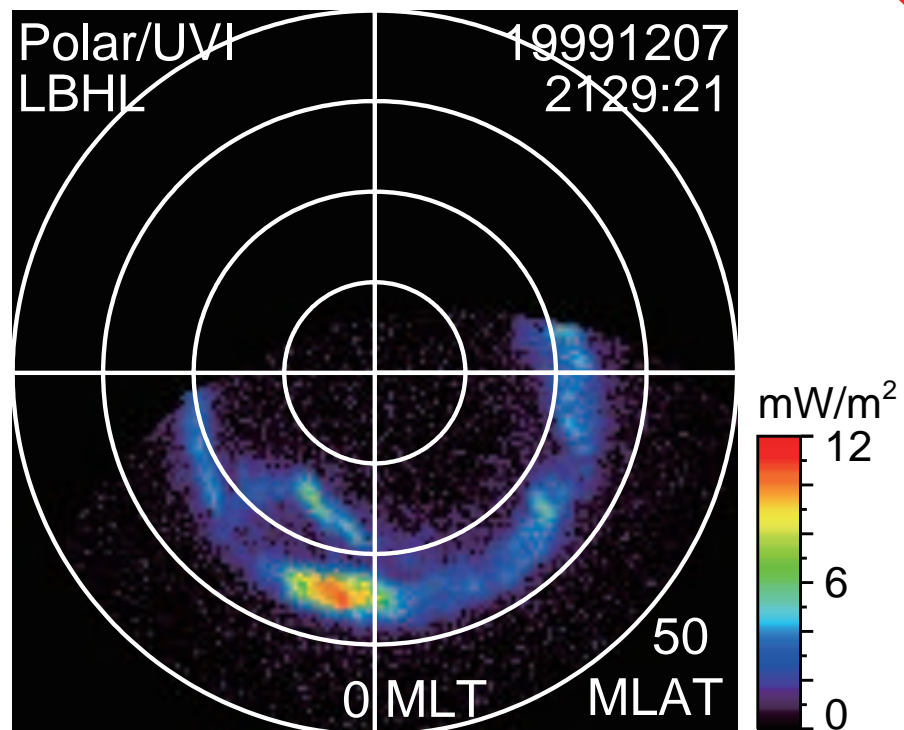
(a1) Satellite (CCD Coord.)



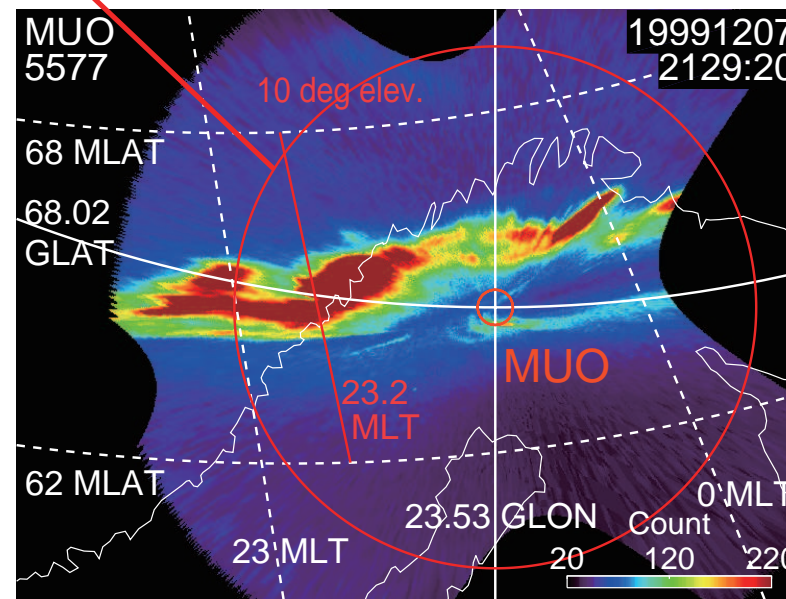
(b1) Ground (CCD Coord.)



(a2) Satellite (Magnetic Coord.)



(b2) Ground (Geodetic Coord.)



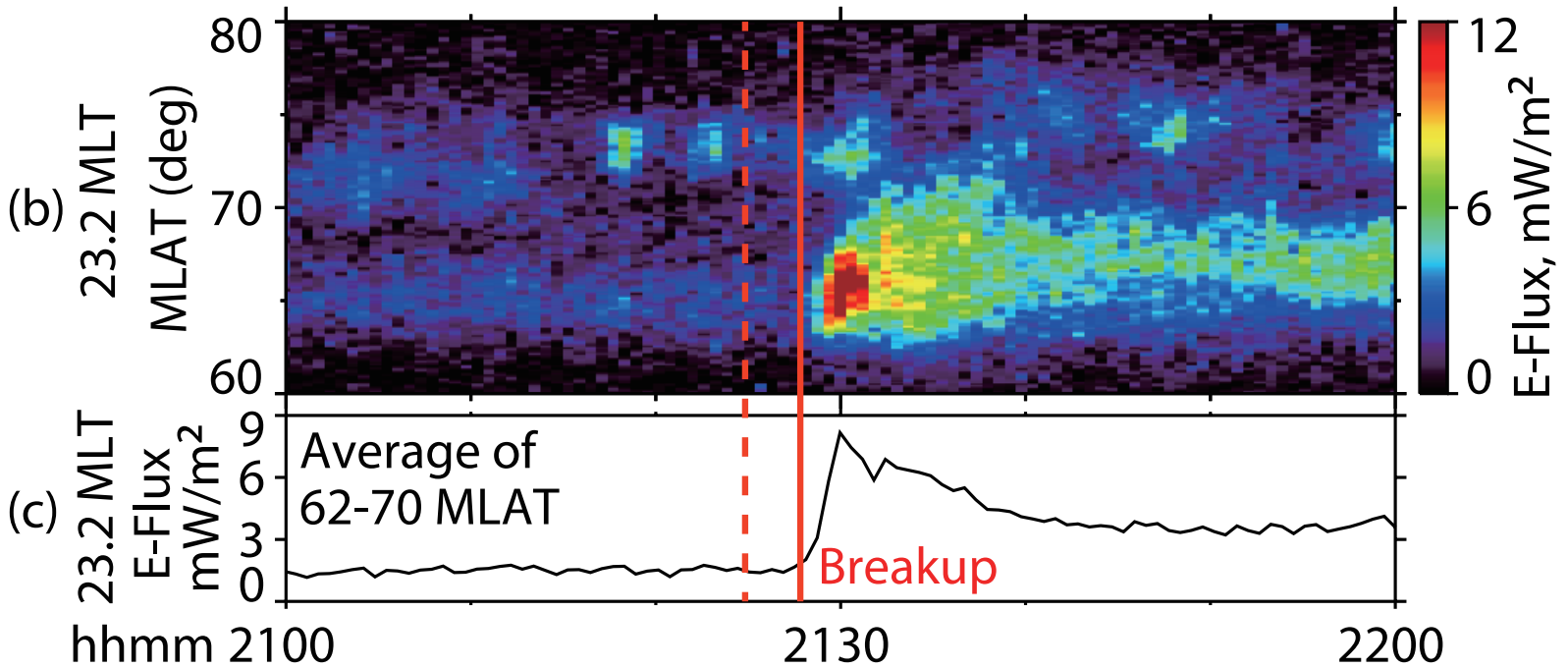
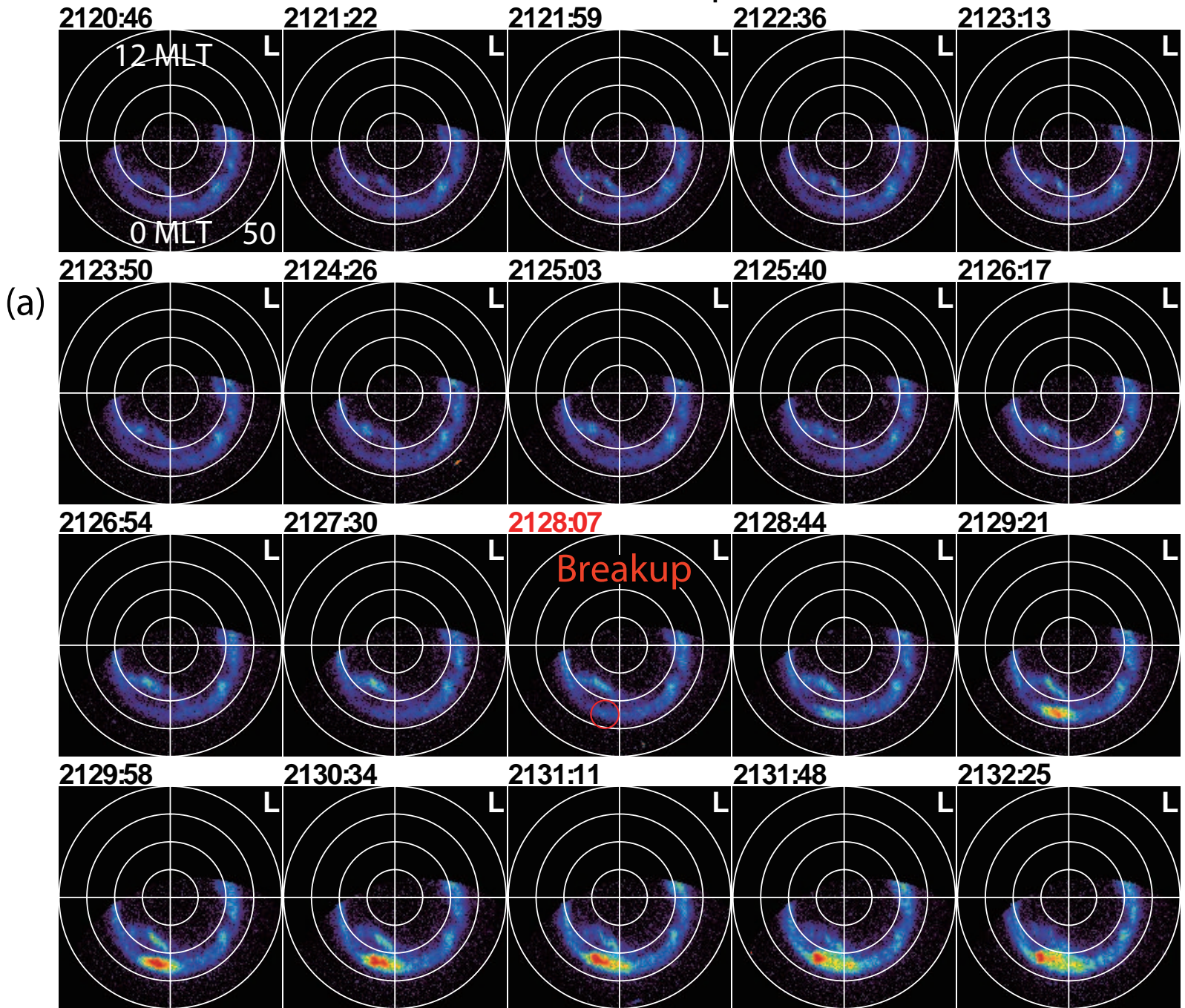
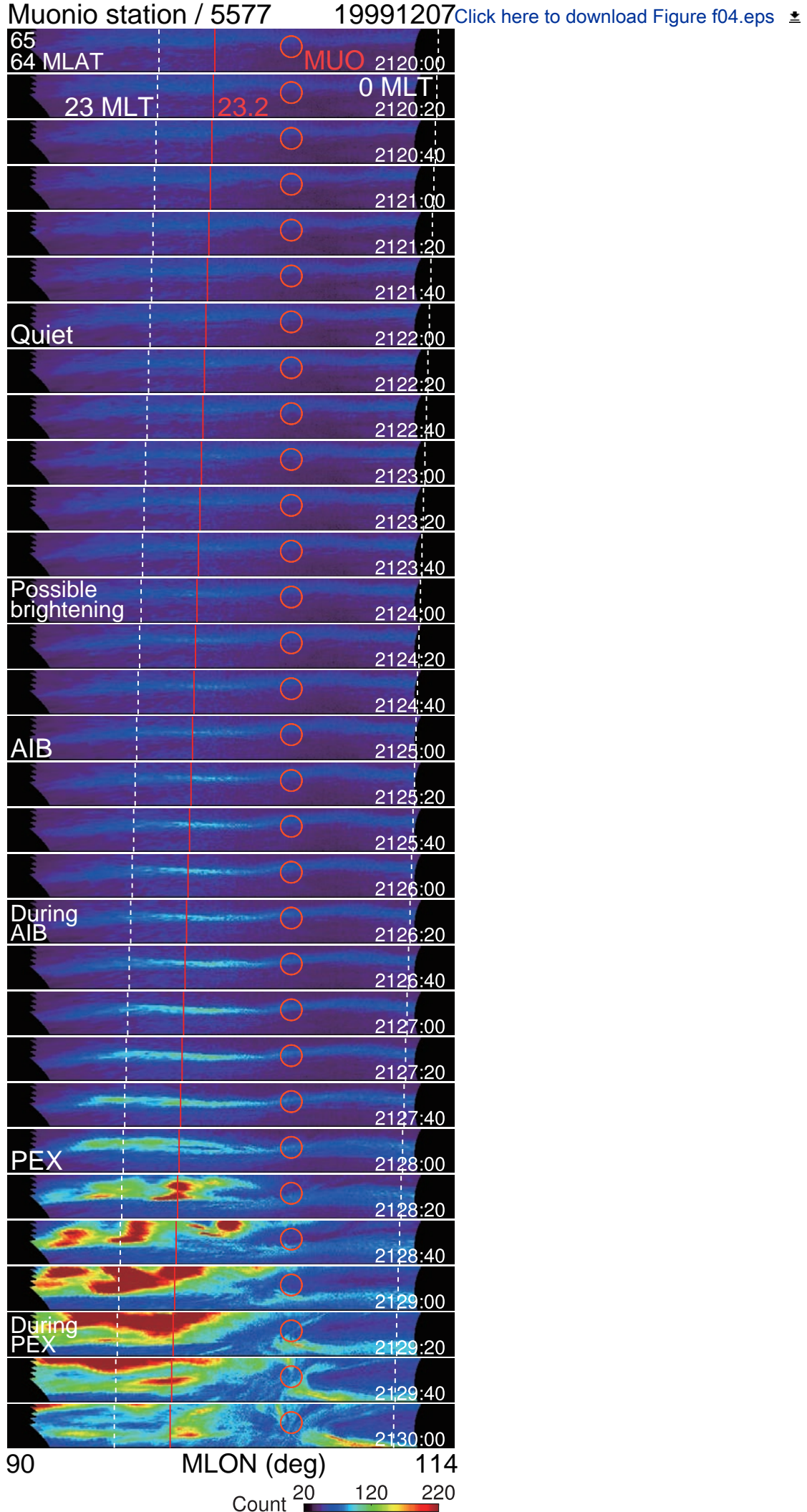
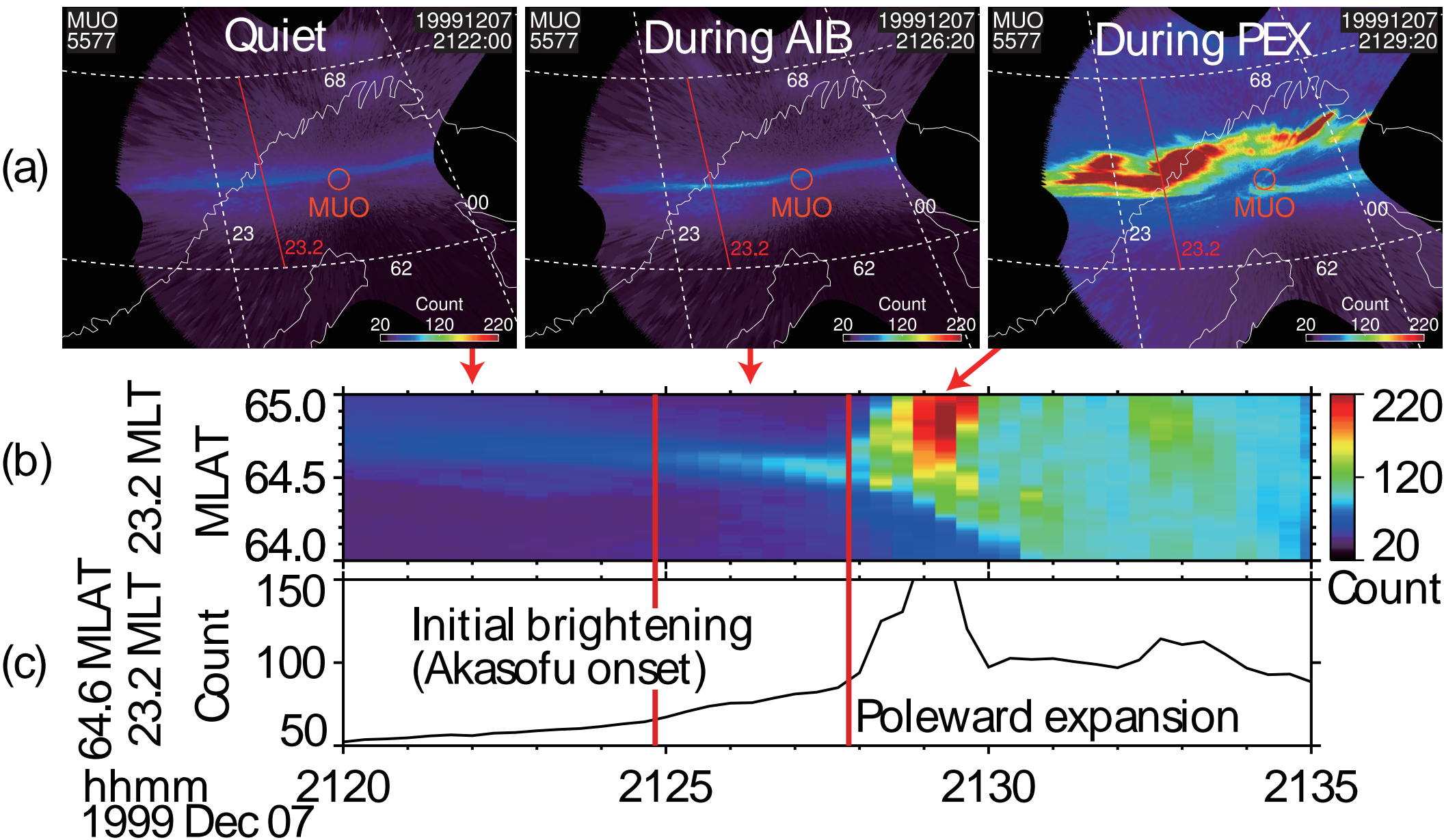
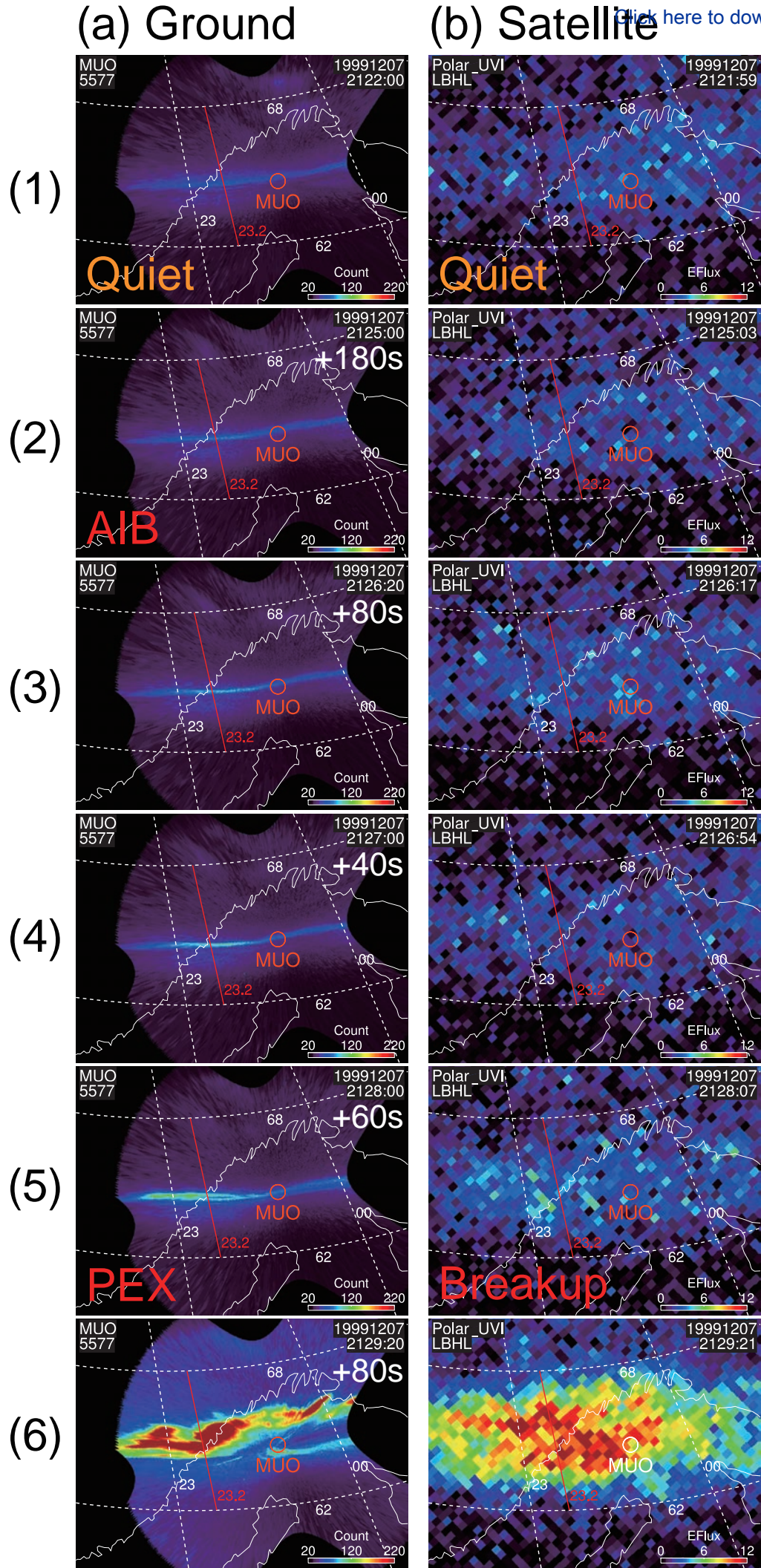


Figure4







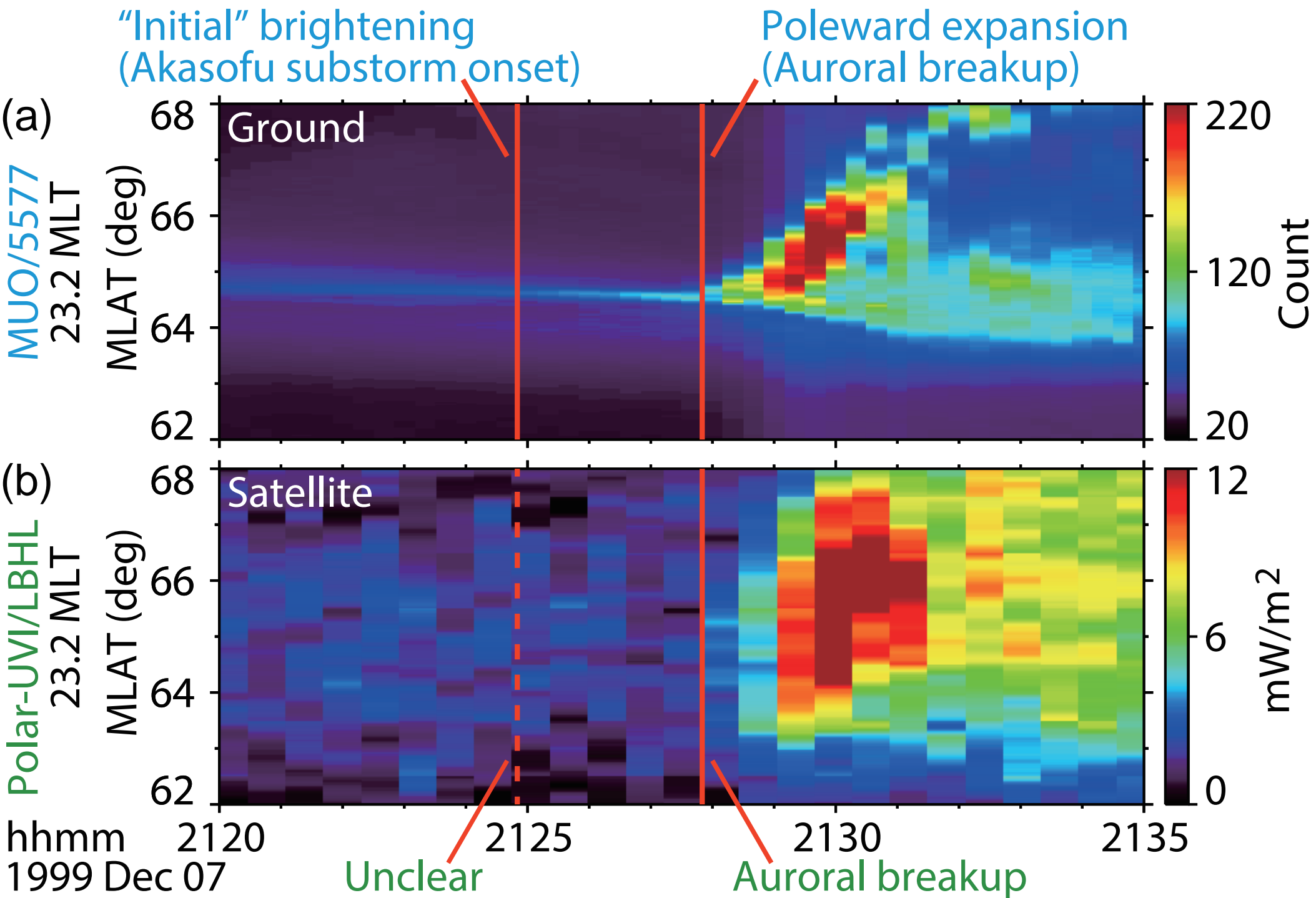
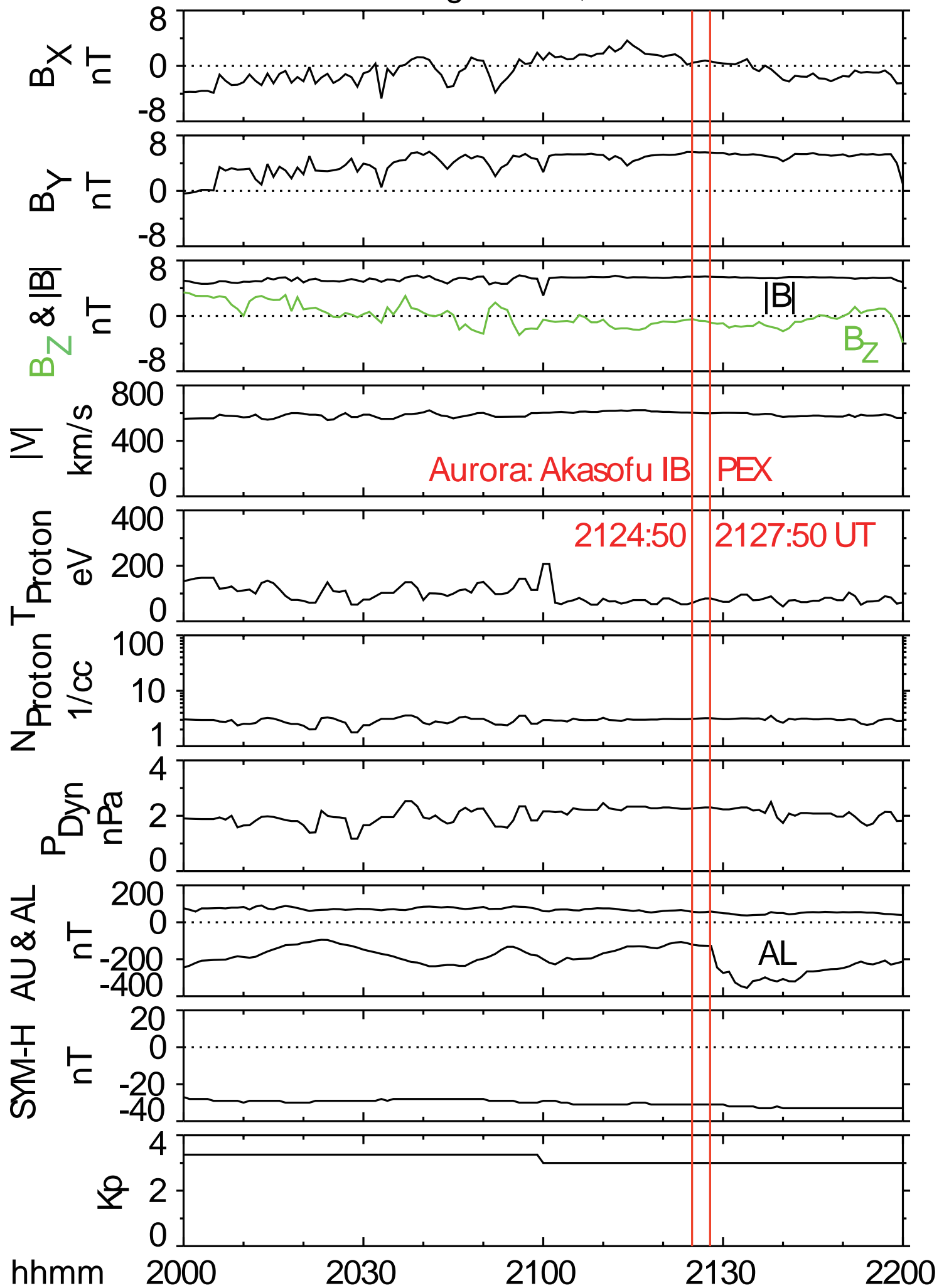
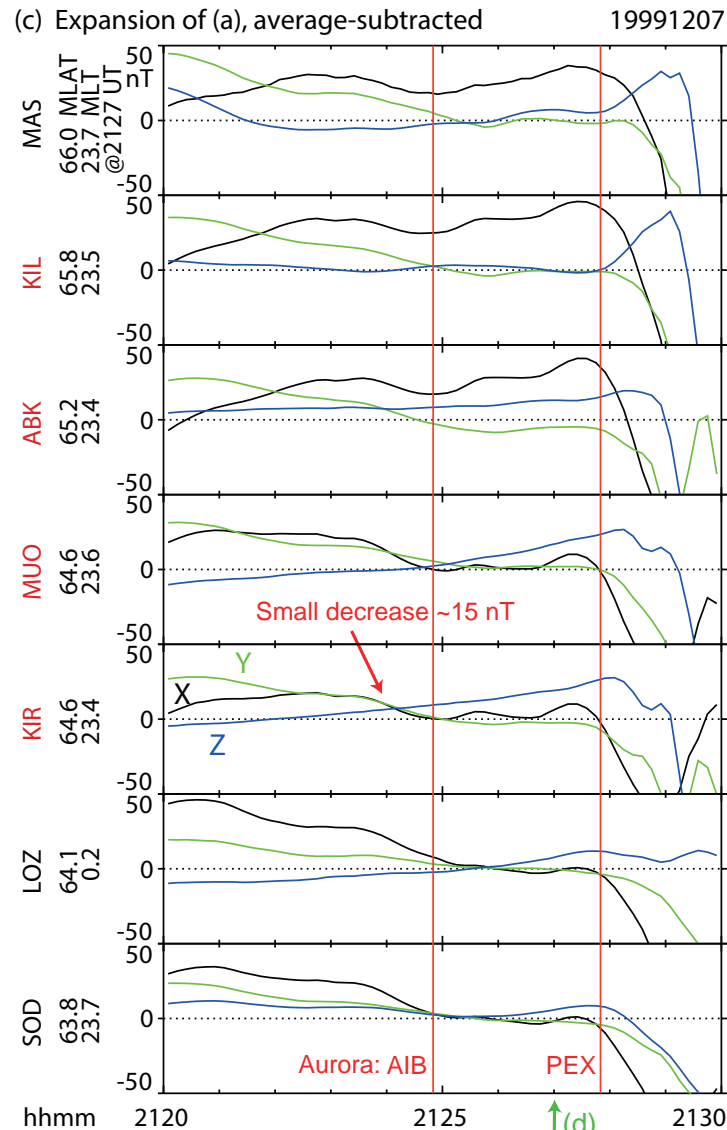
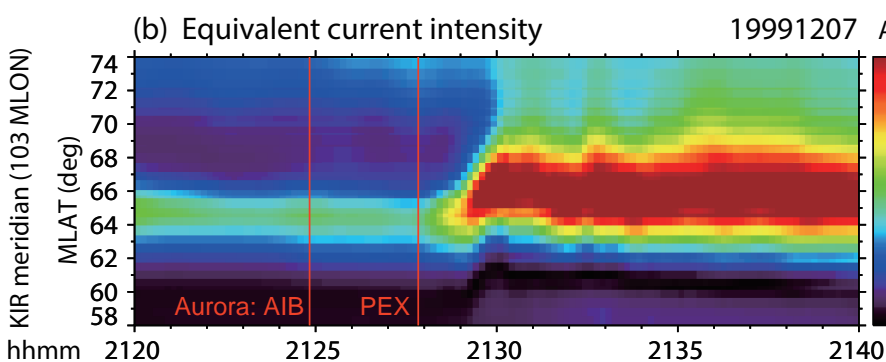
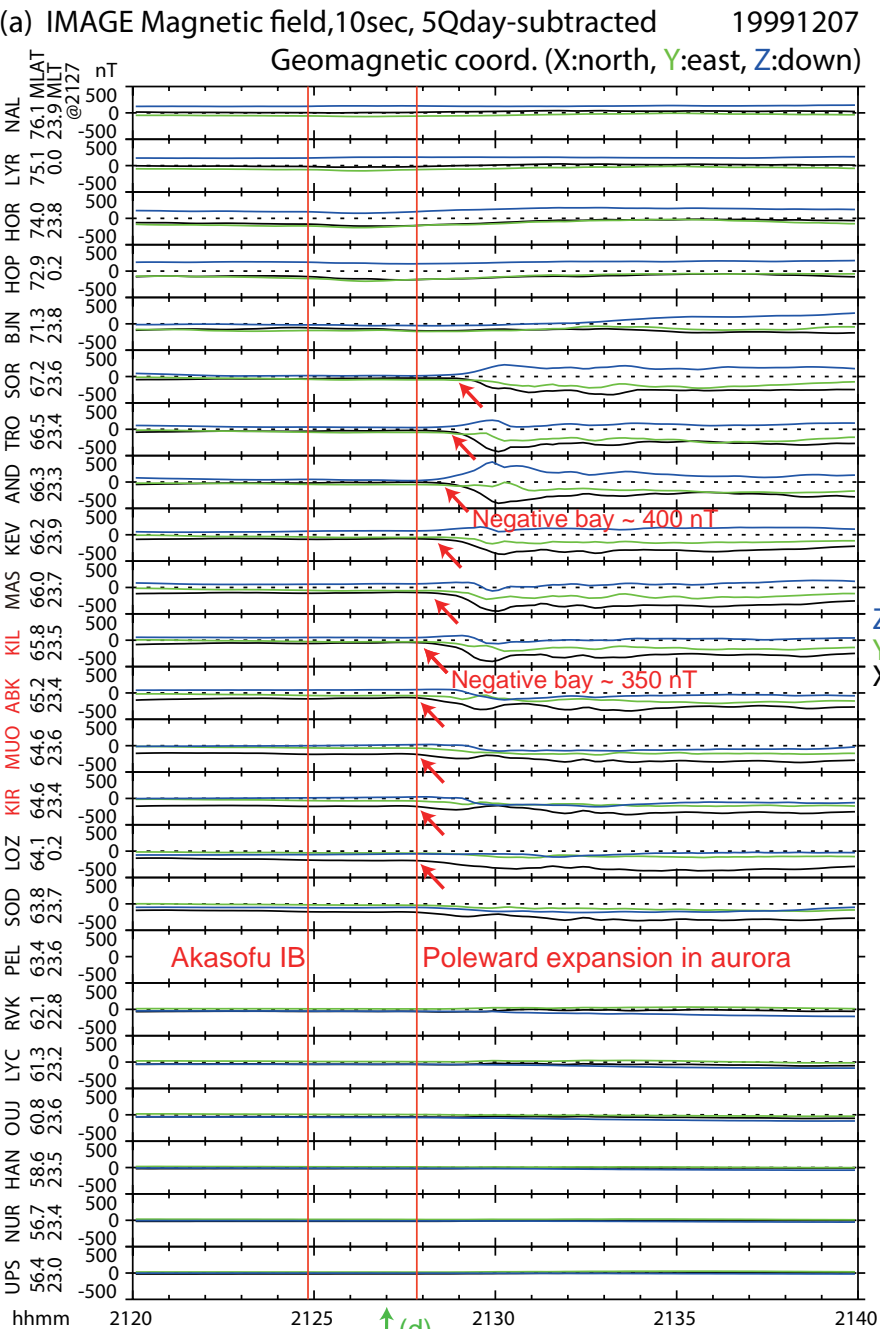


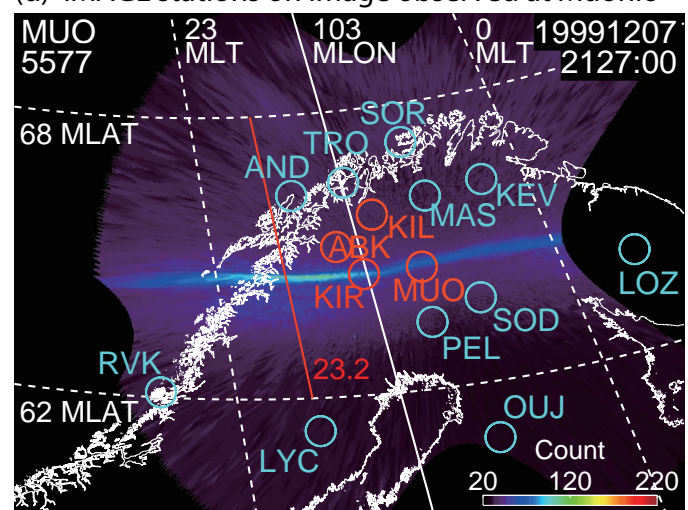
Figure 8

Solar wind & Geomag. indices, OMNI 1min 19991207



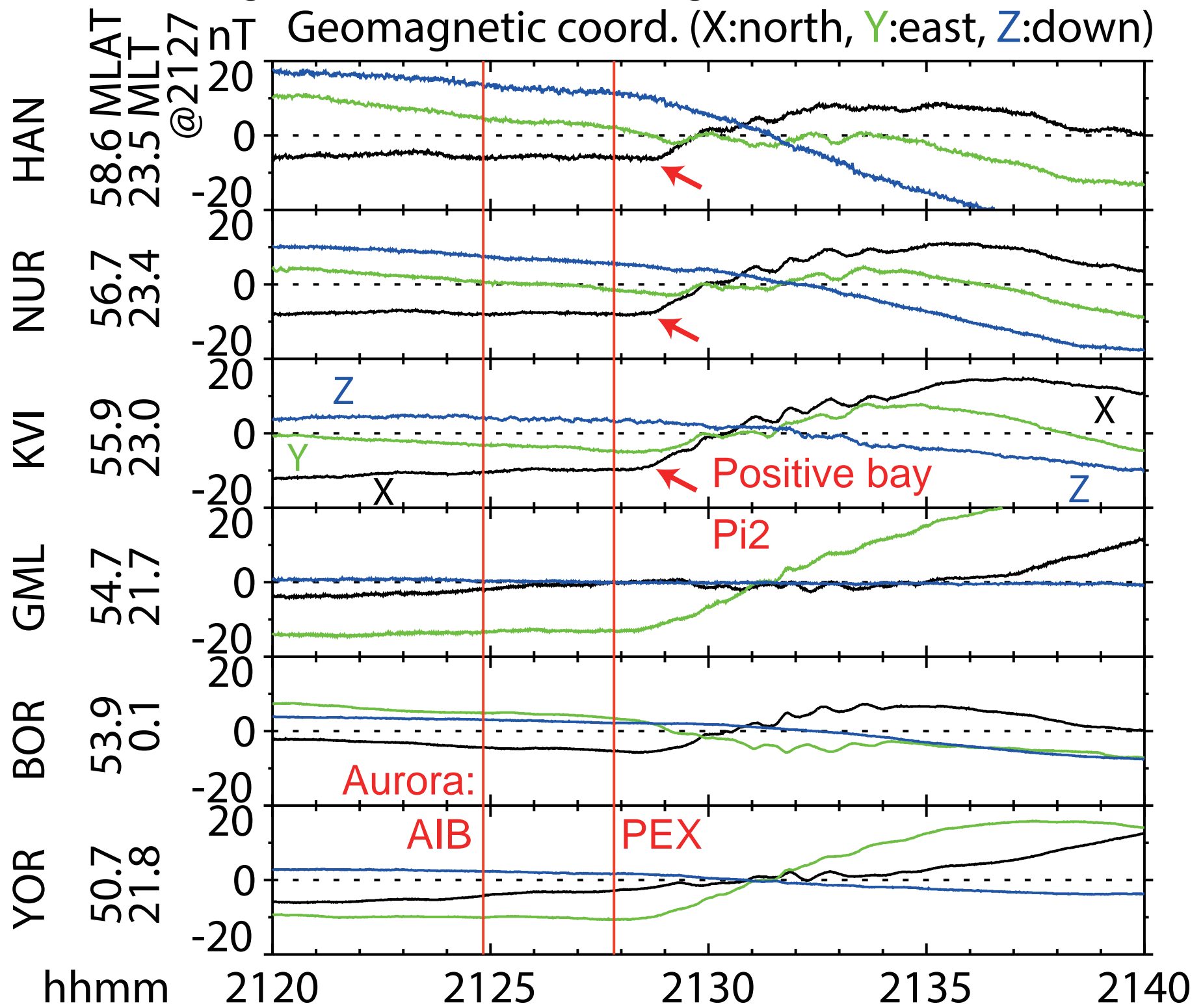


(d) IMAGE stations on image observed at Muonio



SAMNET Magnetic field, 1sec, average-subtracted 19991207

Geomagnetic coord. (X:north, Y:east, Z:down)

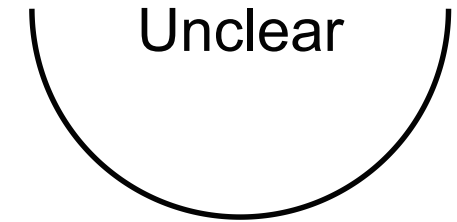
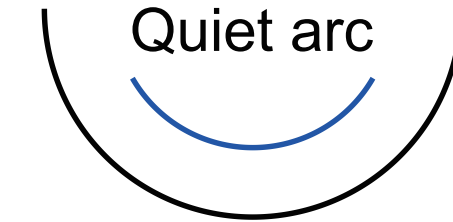


(a) Akasofu (1964)
1 min, ~1 km res.

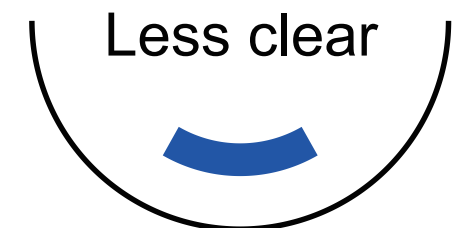
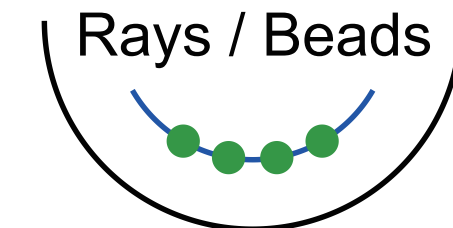
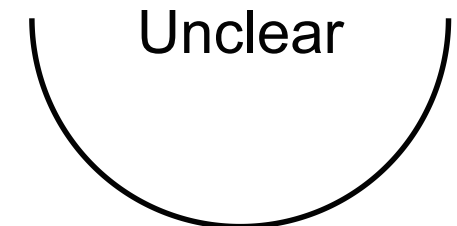
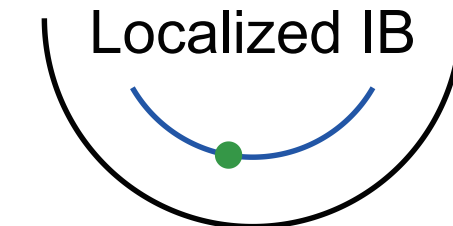
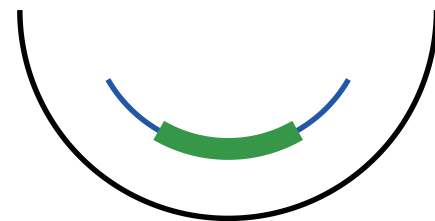
(b) All-sky image
< ~10 sec, ~1 km

(c) Global image
a few min, ~50 km

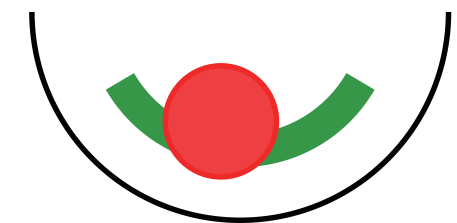
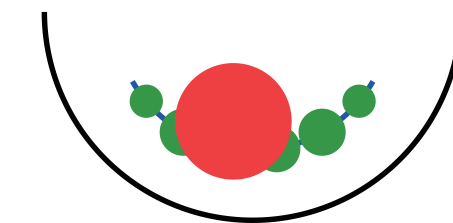
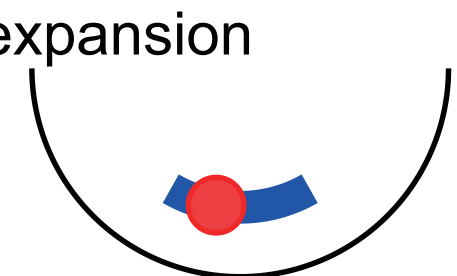
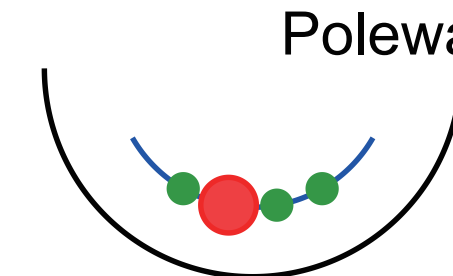
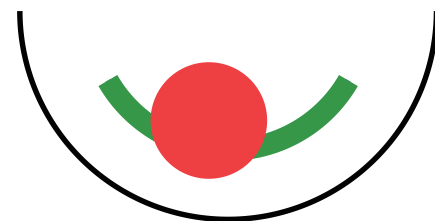
(0) $T < 0$ min
(Quiet arc)



(1) $T = 0-5$ min
(Akasofu
initial
brightening)




(2) $T = 5-10$ min
(Poleward
expansion)



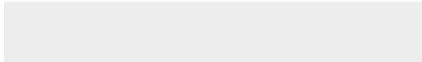



Click here to access/download
Supplementary Material
publis.pdf






Click here to access/download
Supplementary Material
2018ieda_no_url.bib



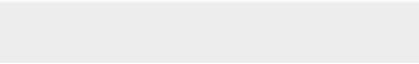



Click here to access/download
Supplementary Material
eps.v2.bbl





Click here to access/download
Supplementary Material
reference_PDF.pdf





Click here to access/download
Supplementary Material
highlighted.pdf



